TABLE I – ALLELIC FREQUENCIES AND GENOTYPE DISTRIBUTIONS (%) OF FGFR4 POLYMORPHISMS IN PROSTATE CANCER PATIENTS, BPH PATIENTS AND MALE CONTROLS

	No.	Gly388Arg FGFR4					rs2011077 FGFR4				
		Allele (Freq)		Genotype (%)			Allele (Freq)		Genotype (%)		
		Arg	Gly	ArgArg	ArgGly	GlyGly	*A*	*G*	*AA*	*GA*	*GG*
Prostate cancer group	492	462 (0.47)	522 (0.53)	133 (27.0)	196 (39.8)	163 (33.1)	511 (0.52)	473 (0.48)	113 (23.0)	285 (57.9)	94 (19.1)
BPH group	165	149 (0.45)	181 (0.55)	42 (25.5)	65 (39.4)	58 (35.2)	197 (0.60)	133 (0.40)	53 (32.1)	91 (55.2)	21 (12.7)
Control group	179	137 (0.38)	221 (0.62)	25 (14.0)	87 (48.6)	67 (37.4)	251 (0.70)	107 (0.30)	83 (46.6)	85 (47.5)	11 (6.1)
Tumor stage											
A	10	7 (0.35)	13 (0.65)	1 (10.0)	5 (50.0)	4 (40.0)	11 (0.55)	9 (0.45)	3 (30.0)	5 (50.0)	2 (20.0)
B	245	224 (0.46)	266 (0.54)	57 (23.3)	110 (44.9)	78 (31.8)	288 (0.59)	202 (0.41)	63 (25.7)	162 (66.1)	20 (8.2)
C	70	55 (0.39)	85 (0.61)	15 (21.4)	25 (35.7)	30 (42.9)	77 (0.55)	63 (0.45)	22 (31.4)	33 (47.1)	15 (21.4)
D1	25	28 (0.56)	22 (0.44)	10 (40.0)	8 (32.0)	7 (28.0)	14 (0.28)	36 (0.72)	3 (12.0)	8 (32.0)	14 (56.0)
D2	142	148 (0.52)	136 (0.48)	50 (35.2)	48 (33.8)	44 (31.0)	121 (0.43)	163 (0.57)	22 (15.5)	77 (54.2)	43 (30.3)
Tumor grade											
Low	15	14 (0.47)	16 (0.53)	4 (26.7)	6 (40.0)	5 (33.3)	21 (0.70)	9 (0.30)	6 (40.0)	9 (60.0)	0 (0.0)
Intermediate	213	193 (0.45)	233 (0.55)	48 (22.5)	97 (45.5)	68 (31.9)	225 (0.54)	195 (0.46)	49 (23.0)	131 (61.5)	33 (15.5)
High	197	189 (0.48)	205 (0.52)	60 (30.5)	69 (35.0)	68 (34.5)	195 (0.49)	199 (0.51)	43 (21.8)	109 (55.3)	45 (22.8)

polymorphisms are presented in Table I. As for the Gly388Arg polymorphism, there was a significant difference in allelic frequency between patients with prostate cancer and controls ($p = 0.005$, Table I), but no significant difference between patients with BPH and controls ($p = 0.067$, Table I). Regarding the rs2011077 polymorphism, there was a significant difference in allelic frequency between patients with prostate cancer and controls ($p < 0.001$, Table I), and between patients with BPH and controls ($p = 0.004$, Table I).

FGFR4 Gly388Arg or rs2011077 genotypes and the risk of prostate cancer or BPH

To evaluate the risk of prostate cancer and BPH according to the *FGFR4* genotypes, logistic regression analysis was conducted with adjustment for age at the time of diagnosis. For the Gly388Arg polymorphism, a significant increased risk of prostate cancer or BPH was found in men with the ArgArg genotype (for prostate cancer: age-adjusted OR [aOR] = 2.207, 95% CI = 1.320–3.690, $p = 0.003$; for BPH: aOR = 1.958, 95% CI = 1.065–3.597, $p = 0.030$) compared with the GlyGly genotype (Table II). For the rs2011077 polymorphism, a significant increased risk of prostate cancer was found in men with the *GG* genotype (aOR = 6.260, 95% CI = 3.152–12.433, $p < 0.001$) or the *GA* genotype (aOR = 2.497, 95% CI = 1.717–3.630, $p < 0.001$) compared with the *AA* genotype. When *GG*, *GA* and *AA* genotypes were valued as 2, 1 and 0, respectively, the presence of the *G* allele was shown to increase the risk of prostate cancer with a gene dosage effect (aOR = 2.500, 95% CI = 1.871–3.339, $p < 0.001$). As for BPH, a significantly increased risk was found in the *GG* genotype (aOR = 3.033, 95% CI = 1.352–6.807, $p = 0.007$) and the *GA* genotype (aOR = 1.700, 95% CI = 1.077–2.683, $p = 0.023$) compared with the *AA* genotype. When *GG*, *GA* and *AA* genotypes were valued as 2, 1 and 0, respectively, the presence of the *G* allele was shown to increase the risk of BPH with a gene dosage effect (aOR = 1.724, 95% CI = 1.218–2.441, $p = 0.002$).

Genotypes of FGFR4 Gly388Arg or rs2011077 polymorphisms and disease status of prostate cancer

We examined the relationship between FGFR4 Gly388Arg or rs2011077 polymorphisms and the prostate tumor stage or grade at the time of diagnosis (Table II). Regarding the tumor stage and the Gly388Arg polymorphism, patients with prostate cancer with the ArgArg genotype had a 1.804-fold increased risk of metastatic prostate cancer ($p = 0.015$) compared with the GlyGly genotype. For the rs2011077 polymorphism, patients with prostate cancer with the *GG* genotype had a 5.550-fold increased risk of metastatic prostate cancer ($p < 0.001$) compared with the *AA* genotype. There was no statistically significant result between Gly388Arg or rs2011077 polymorphisms and the prostate cancer grade.

Genotypes of FGFR4 Gly388Arg or rs2011077 polymorphisms and prognosis of prostate cancer

Of the 492 patients with prostate cancer, cancer-specific survival and disease-free survival data were available in 117 patients of Stage D2 and in 141 patients of Stages A–D1, respectively. Regarding cancer-specific survival from prostate cancer and the two polymorphisms, there was no statistical significance among the different genotype groups of the Gly388Arg ($p = 0.313$) (Fig. 1) or rs2011077 ($p = 0.852$) polymorphisms. There was also no statistical significance regarding disease-free survival and the Gly388Arg ($p = 0.840$) (Fig. 2) or rs2011077 ($p = 0.971$) polymorphism.

Linkage disequilibrium between Gly388Arg and rs2011077 polymorphisms

The *D'* values of the group that had patients with prostate cancer, the group that had patient with BPH and controls were 0.471, 0.657 and 0.849, respectively.

TABLE II – STATISTICAL ANALYSES RESULTS OF THE GENOTYPE FREQUENCY

	Gly388Arg polymorphism aOR (95% CI, *p*)			rs2011077 polymorphism aOR (95% CI, *p*)		
	GlyGly	GlyArg	ArgArg	*AA*	*GA*	*GG*
Study group						
Prostate cancer *versus* control	1	0.939 (0.641–1.375, 0.747)	2.207 (1.320–3.690, 0.003)	1	2.497 (1.717–3.630, <0.001)	6.260 (3.152–12.433, <0.001)
BPH *versus* control	1	0.871 (0.540–1.404, 0.570)	1.958 (1.065–3.597, 0.030)	1	1.700 (1.077–2.683, 0.023)	3.033 (1.352–6.807, 0.007)
Tumor stage						
Stage D *versus* Stage A + B + C	1	0.867 (0.550–1.366, 0.539)	1.804 (1.120–2.906, 0.015)	1	1.492 (0.894–2.491, 0.126)	5.550 (3.016–10.214, <0.001)
Tumor grade						
High *versus* Low + Intermediate	1	0.722 (0.460–1.132, 0.156)	1.237 (0.753–2.035, 0.401)	1	1.003 (0.626–1.608, 0.989)	1.757 (0.963–1.016, 0.066)

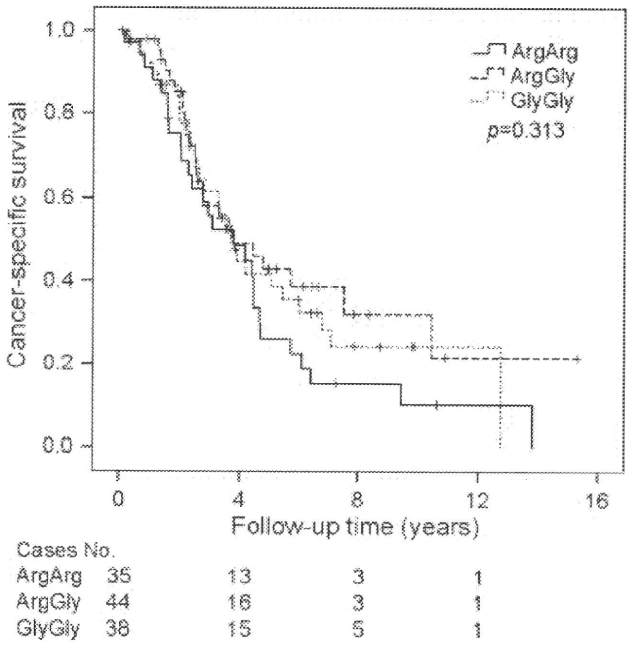

FIGURE 1 – Genotypes of Gly388Arg and the cancer-specific survival of Stage D2 prostate cancer.

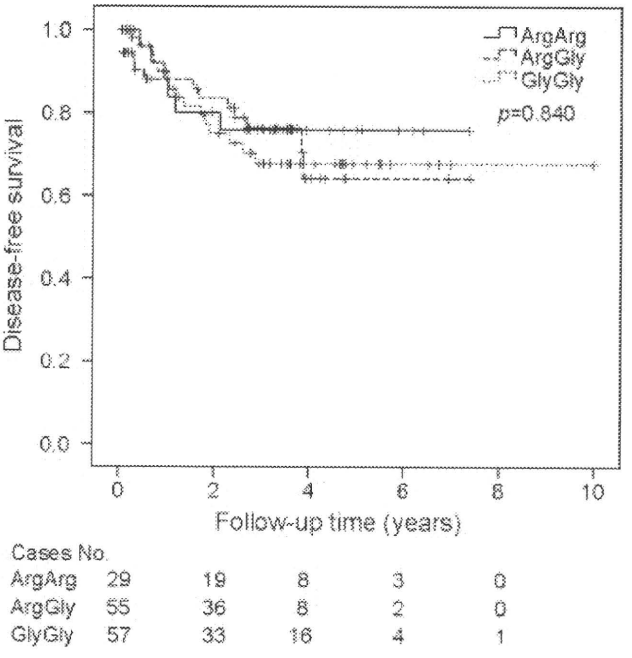

FIGURE 2 – Genotypes of Gly388Arg and the disease-free survival of Stage A–D1 prostate cancer.

Discussion

The present study showed a significant association between the Arg allele of the *FGFR4* Gly388Arg polymorphism and the development and progression of prostate cancer in a native Japanese male population. Our results further indicate that the Arg allele had a recessive effect on the development and progression of prostate cancer (Table II). These results are in line with a study on prostate cancer in whites and African-Americans by Wang *et al.*[10] However, it is noticeable that although the risk of prostate cancer

in the Japanese population was the lowest among the 3 races, the Arg388 allele frequency in the Japanese population was the highest among patients with prostate cancer from the 3 races, whereas the African-Americans had a contradictory result (0.47 in the Japanese population in our study, 0.36 in whites and 0.12 in African-Americans in Wang *et al.*'s study[10]). This suggests that other environmental or genetic factors must influence the effects of the FGFR4 Arg388 allele.

Although there is no direct biological relationship between prostate cancer and BPH, it is well conceivable that genetic polymorphisms affecting levels of growth factors, including FGFR4, may have a significant impact on both prostate cancer and BPH, because both disease conditions are under the influence of common growth factors. Normal growth patterns in the prostate may result not only from increased cell proliferation but also from decreased levels in programmed cell death.[23] Any imbalance between the physiological process of cell proliferation and cell death may lead to changes in prostate size with the subsequent development of abnormalities in the gland. In the present study, patients with BPH were excluded from the control group to eliminate the confounding effect of the *FGFR4* polymorphism, and we found that men with the ArgArg genotype have a 1.958-fold increased risk of developing BPH ($p = 0.030$) compared with men with the GlyGly genotype. In addition, Bange *et al.*[12] reported that the Arg388 allele was associated with progression in patients with colon cancer. Stadler *et al.*[24] found that FGFR4 Gly388 could reduce a breast cancer cell line response to lysophosphatidic acid (LPA) by downregulating the LPA receptor Edg-2. LPA plays an important role in activation of the mitogenic extracellular signal-regulated kinase (ERK) pathway and in regulating mitogenic signaling and the growth of prostate cancer cells.[25] More recently, Sahadevan *et al.*[11] reported that FGFR4 may be an important target to disrupt FGF signaling in prostate cancer. Taken together, it suggested that FGFR4 Arg388 could enhance the development of prostate cancer and BPH by upregulating LPA signaling, which promotes mitosis mediated by ERK. On the other hand, Wang *et al.*[26] found that Ehm2 expression was upregulated in prostate cancer cell lines and prostate cancer tissues, and the expression of the Arg388 of FGFR4 resulted in increased Ehm2 expression, which may lead to decreased adhesion to Collagen IV; so, Arg388 may be associated with the metastatic phenotype in cancers.[27] Furthermore, Wang *et al.*[10] reported that the expression of *FGFR4* Arg388 in immortalized prostate epithelial cells resulted in increased cell motility and invasion and upregulation of the urokinase-type plasminogen activator receptor, which is known to promote invasion and metastasis.[28] These may explain the relationship between the Arg388 of FGFR4 and the increased metastatic disease status of prostate cancer observed in the present study.

The Gly388Arg polymorphism lies in the transmembrane domain of FGFR4. Mutations in the transmembrane domains of TKRs have been implicated in the induction of pathological phenotypes. These mutations are believed to stabilize TKR dimers, and thus promote unregulated signaling. For example, achondroplasia is often attributed to a Gly388Arg mutation in the transmembrane domain of FGFR3.[29] To further explore the association of the polymorphism of the transmembrane domain of FGFR4 and the risk of prostate cancer and BPH, we searched for common polymorphisms around the Gly388Arg polymorphism in the NCBI SNP database literature. As a result, the rs2011077 polymorphism in intron 11 was found, which had 0.471 frequency and 1,213 base distance to the Gly388Arg polymorphism. We found that the *G* allele was more frequently found in patients with prostate cancer and in patients with BPH, and it might increase the risk of prostate cancer and BPH with a gene dosage effect (Table II). The present data suggested that the Gly388Arg polymorphism and rs2011077 polymorphism were in strong linkage disequilibrium and tightly linked in controls; however, they were not in tight linkage in the group that had patients with prostate cancer. This was in line with the results that the *G* allele of the rs2011077 polymorphism had a gene dosage effect on the development of prostate cancer and BPH, yet the Arg allele seemed to have a recessive influence. Although the rs2011077 polymorphism is located in the intron, it remains unknown whether it may have any significant biological effect on FGFR4 protein or the *FGFR4* expression level. In addition, the polymorphism might be in strong linkage disequilibrium with other unknown polymorphisms, which have a significant biological influence on prostate cancer and BPH development.

Although our study showed that the Arg388 allele and the *G* allele of the rs2011077 polymorphism of FGFR4 was associated with the advanced status of prostate cancer, no relationship was observed between polymorphisms of FGFR4 and the prognosis of prostate cancer, which seemed contrary to the results of several studies that the Arg388 allele of FGFR4 was associated with the prognosis of various cancers.[10,12,14–16] This might be due to the influence of other factors on the prognosis of prostate cancer, one of which is the complexity of the FGFR4 signaling pathway. Studies on the role of FGFR4 in carcinogenesis provide evidence for the complexity of the FGF/FGFR signaling pathway in different tumor types.[30,31] This complexity was reflected to some degree by the contradictory results of the relationship between the Gly388Arg polymorphism and the prognosis of several cancers,[15,16,18,19] and even the same cancers, although other factors might be involved. For localized prostate cancer, clinicopathologic characteristics, such as the Gleason score and the status of the surgical margin, may mask the relationship between polymorphisms of FGFR4 and the prognosis of prostate cancer. In addition, most patients with prostate cancer of Stage D2 and some patients with prostate cancer of Stage A–D1 in our study received androgen deprivation therapies (ADT). It has been demonstrated that genetic polymorphisms can influence tumor response and the severity of adverse effects of chemotherapy.[32–34] Our recent data showed that IGF-I and CYP19 polymorphisms had a significant impact on the prognosis of patients of Stage D2, suggesting that some genetic factors are related to the progression of bone metastasis, hormone-independent growth of tumor cells or the response to ADT.[35] Therefore, other polymorphisms may mask the relationship between polymorphisms of FGFR4 and the prognosis of Stage D2 prostate cancer. All of these factors may cloud the cancer prognosis.

In conclusion, the present results indicate that the Arg allele of Gly388Arg polymorphism and the G allele of rs2011077 polymorphism in the transmembrane domain of *FGFR4* have a significant impact on the development of prostate cancer and BPH, and the progression of prostate cancer in Japanese men. Further studies with extensive haplotype analyses are warranted to delineate the significance of each haplotype of the *FGFR4* locus containing the 2 polymorphisms in more Japanese subjects and other racial-ethnic groups.

Acknowledgements

We are indebted to the many physicians and urologists of the Akita University Medical Center and other community hospitals for providing samples and clinical information. We greatly thank Ms. Mitobe and Ms. Fujiwara for their technical assistance.

References

1. Jemal A, Siegel R, Ward E, Murray T, Xu J, Smigal C, Thun MJ. Cancer statistics, 2006. CA Cancer J Clin 2006;56:106–30.
2. Parkin DM, Whelan SL, Ferlay J, Teppo L, Thomas DB, eds. Cancer incidence in five continents, vol. VIII. Lyon, France: IARC Scientific Publications, 2002;1–781.
3. Penson DF, Chan JM. Prostate cancer. J Urol 2007;177:2020–9.
4. Wakai K. Descriptive epidemiology of prostate cancer in Japan and Western countries (in Japanese). Nippon Rinsho 2005;63:207–12.
5. Oishi K, Yoshida O, Schroeder FH. The geography of prostate cancer and its treatment in Japan. Cancer Surv 1995;23:267–80.

6. McCracken M, Olsen M, Chen MS, Jr, Jemal A, Thun M, Cokkinides V, Deapen D, Ward E. Cancer incidence, mortality, and associated risk factors among Asian Americans of Chinese, Filipino, Vietnamese, Korean, and Japanese ethnicities. CA Cancer J Clin 2007;57: 190–205.
7. Powers CJ, McLeskey SW, Wellstein A. Fibroblast growth factors, their receptors and signaling. Endocr Relat Cancer 2000;7:165–97.
8. Ropiquet F, Giri D, Kwabi-Addo B, Mansukhani A, Ittmann M. Increased expression of fibroblast growth factor 6 in human prostatic intraepithelial neoplasia and prostate cancer. Cancer Res 2000;60: 4245–50.
9. Kwabi-Addo B, Ropiquet F, Giri D, Ittmann M. Alternative splicing of fibroblast growth factor receptors in human prostate cancer. Prostate 2001;46:163–72.
10. Wang J, Stockton DW, Ittmann M. The fibroblast growth factor receptor-4 Arg388 allele is associated with prostate cancer initiation and progression. Clin Cancer Res 2004;10:6169–78.
11. Sahadevan K, Darby S, Leung H, Mathers M, Robson C, Gnanapragasam V. Selective over-expression of fibroblast growth factor receptors 1 and 4 in clinical prostate cancer. J Pathol 2007;213:82–90.
12. Bange J, Prechtl D, Cheburkin Y, Specht K, Harbeck N, Schmitt M, Knyazeva T, Muller S, Gartner S, Sures I, Wang H, Imyanitov E, et al. Cancer progression and tumor cell motility are associated with the FGFR4 Arg(388) allele. Cancer Res 2002;62:840–7.
13. Spinola M, Leoni VP, Tanuma J, Pettinicchio A, Frattini M, Signoroni S, Agresti R, Giovanazzi R, Pilotti S, Bertario L, Ravagnani F, Dragani TA. FGFR4 Gly388Arg polymorphism and prognosis of breast and colorectal cancer. Oncol Rep 2005;14:415–9.
14. da Costa Andrade VC, Parise O, Jr, Hors CP, de Melo Martins PC, Silva AP, Garicochea B. The fibroblast growth factor receptor 4 (FGFR4) Arg388 allele correlates with survival in head and neck squamous cell carcinoma. Exp Mol Pathol 2007;82:53–7.
15. Morimoto Y, Ozaki T, Ouchida M, Umehara N, Ohata N, Yoshida A, Shimizu K, Inoue H. Single nucleotide polymorphism in fibroblast growth factor receptor 4 at codon 388 is associated with prognosis in high-grade soft tissue sarcoma. Cancer 2003;98:2245–50.
16. Spinola M, Leoni V, Pignatiello C, Conti B, Ravagnani F, Pastorino U, Dragani TA. Functional FGFR4 Gly388Arg polymorphism predicts prognosis in lung adenocarcinoma patients. J Clin Oncol 2005; 23:7307–11.
17. Streit S, Mestel DS, Schmidt M, Ullrich A, Berking C. FGFR4 Arg388 allele correlates with tumour thickness and FGFR4 protein expression with survival of melanoma patients. Br J Cancer 2006;94: 1879–86.
18. Matakidou A, El Galta R, Rudd MF, Webb EL, Bridle H, Eisen T, Houlston RS. Further observations on the relationship between the FGFR4 Gly388Arg polymorphism and lung cancer prognosis. Br J Cancer 2007;96:1904–7.
19. Yang YC, Lu ML, Rao JY, Wallerand H, Cai L, Cao W, Pantuck A, Dalbagni G, Reuter V, Figlin RA, Belldegrun A, Cordon-Cardo C, et al. Joint association of polymorphism of the FGFR4 gene and mutation TP53 gene with bladder cancer prognosis. Br J Cancer 2006;95: 1455–8.
20. Sanda MG, Beaty TH, Stutzman RE, Childs B, Walsh PC. Genetic susceptibility of benign prostatic hyperplasia. J Urol 1994;152:115–9.
21. Boget S, Cereser C, Parvaz P, Leriche A, Revol A. Fibroblast growth factor receptor 1 (FGFR1) is over-expressed in benign prostatic hyperplasia whereas FGFR2-IIIc and FGFR3 are not. Eur J Endocrinol 2001;145:303–10.
22. Kuriyama M, Akimoto S, Akaza H, Arai Y, Usami M, Imai K, Tanaka Y, Yamazaki H, Kawada Y, Koiso K, et al. Comparison of various assay systems for prostate-specific antigen standardization. Jpn J Clin Oncol 1992;22:393–9.
23. Isaacs JT, Coffey DS. Etiology and disease process of benign prostatic hyperplasia. Prostate 1989;2:33–50.
24. Stadler CR, Knyazev P, Bange J, Ullrich A. FGFR4 GLY388 isotype suppresses motility of MDA-MB-231 breast cancer cells by EDG-2 gene repression. Cell Signal 2006;18:783–94.
25. Daaka Y. Mitogenic action of LPA in prostate. Biochim Biophys Acta 2002;1582:265–9.
26. Wang J, Cai Y, Penland R, Chauhan S, Miesfeld RL, Ittmann M. Increased expression of the metastasis-associated gene Ehm2 in prostate cancer. Prostate 2006;66:1641–52.
27. Shimizu K, Nagamachi Y, Tani M, Kimura K, Shiroishi T, Wakana S, Yokota J. Molecular cloning of a novel NF2/ERM/4.1 superfamily gene, ehm2, that is expressed in high-metastatic K1735 murine melanoma cells. Genomics 2000;65:113–20.
28. Sidenius N, Blasi F. The urokinase plasminogen activator system in cancer: recent advances and implication for prognosis and therapy. Cancer Metastasis Rev 2003;22:205–22.
29. Shiang R, Thompson LM, Zhu YZ, Church DM, Fielder TJ, Bocian M, Winokur ST, Wasmuth JJ. Mutations in the transmembrane domain of FGFR3 cause the most common genetic form of dwarfism, achondroplasia. Cell 1994;78:335–42.
30. Cavallaro U, Niedermeyer J, Fuxa M, Christofori G. N-CAM modulates tumour-cell adhesion to matrix by inducing FGF-receptor signalling. Nat Cell Biol 2001;3:650–7.
31. Shah RN, Ibbitt JC, Alitalo K, Hurst HC. FGFR4 overexpression in pancreatic cancer is mediated by an intronic enhancer activated by HNF1alpha. Oncogene 2002;21:8251–61.
32. Xiao Z, Yang L, Xu Z, Zhang Y, Liu L, Nie L, Li L, Wang J, Hao Y. Glutathione S-transferases (GSTT1 and GSTM1) genes polymorphisms and the treatment response and prognosis in Chinese patients with de novo acute myeloid leukemia. Leuk Res 2008;32:1288–91.
33. Mossallam GI, Abdel Hamid TM, Samra MA. Glutathione S-transferase GSTM1 and GSTT1 polymorphisms in adult acute myeloid leukemia; its impact on toxicity and response to chemotherapy. J Egypt Natl Cancer Inst 2006;18:264–73.
34. Matsui T, Omura K, Kawakami K, Morita S, Sakamoto J. Genotype of thymidylate synthase likely to affect efficacy of adjuvant 5-FU based chemotherapy in colon cancer. Oncol Rep 2006;16:1111–5.
35. Tsuchiya N, Wang L, Suzuki H, Segawa T, Fukuda H, Narita S, Shimbo M, Kamoto T, Mitsumori K, Ichikawa T, Ogawa O, Nakamura A, et al. Impact of IGF-I and CYP19 gene polymorphisms on the survival of patients with metastatic prostate cancer. J Clin Oncol 2006;24:1982–9.

Original Research

Usefulness of Apparent Diffusion Coefficient Map in Diagnosing Prostate Carcinoma: Correlation with Stepwise Histopathology

Kengo Yoshimitsu, MD,[1]* Keijiro Kiyoshima, MD,[2] Hiroyuki Irie, MD,[1] Tsuyoshi Tajima, MD,[1] Yoshiki Asayama, MD,[1] Masakazu Hirakawa, MD,[1] Kousei Ishigami, MD,[1] Seiji Naito, MD,[3] and Hiroshi Honda, MD[1]

Purpose: To elucidate the performance of apparent diffusion coefficient (ADC) map in localizing prostate carcinoma (PC) using stepwise histopathology as a reference.

Materials and Methods: Preoperative MR images of 37 patients with PC who had undergone radical prostatectomy were retrospectively evaluated. First, T2-weighted images (T2WI) alone were interpreted (T2WI reading), and then T2WI along with ADC map were interpreted (T2WI/ADC map reading). Sextant-based sensitivity and specificity, and the ratio of the detected volume to the whole tumor volume (% tumor volume) were compared between the two interpretations, and results were also correlated to Gleason's scores (GS). ADC values were correlated to histological grades.

Results: Sensitivity was significantly higher in T2WI/ADC map reading than in T2WI reading (71% vs. 51%), but specificity was similar (61% vs. 60%). By adding ADC map to T2WI, % tumor volume detected increased significantly in transitional zone (TZ) lesions, but not in peripheral zone (PZ) lesions. % tumor volume detected with T2WI/ADC map reading showed a positive correlation with GS of the specimens. Less differentiated PC were associated with lower ADC values and higher detectability.

Conclusion: T2WI/ADC map reading was better than T2WI reading in PC detection and localization. This approach may be particularly useful for detecting TZ lesions and biologically aggressive lesions.

Key Words: prostate carcinoma; MR; diffusion-weighted image; ADC map; localization
J. Magn. Reson. Imaging 2008;27:132–139.

PROSTATE CARCINOMA (PC) is one of the most common malignancies in males, and it accounts for approximately 30,000 new annual deaths in the United States (1). To date, surgical resection of the whole organ has been the only method of eradicating this type of malignancy; however, less invasive alternative local therapies, including intensive modulated radiation therapy (IMRT), high-intensity focused ultrasound (HIFU), and brachytherapy, are being introduced due to the increasing clinical demand for the preservation of functional aspects of the prostate and related organs (2–4).

The current role of MRI in the diagnosis of PC is primarily based on T2-weighted images (T2WI), and this approach has remained relatively limited in terms of usefulness, as it can mainly be used to determine whether or not a lesion extends beyond the confinement of the organ capsule (5), a measure used for determining the indication for radical prostatectomy. Also, in the cases of the less invasive local therapies mentioned above, the current approach is to cover the whole organ, regardless of the location or bulk of the tumor within the organ, provided extracapsular extension of the tumor has been excluded (2–4). Because PC can be multifocal and involve any part of the organ, more precise localization and focal targeting of lesions may be beneficial for patients, potentially rendering retreatment for the recurrent tumors possible, in addition to maximizing the options for the preservation of function.

Various MR approaches have been investigated and applied to localize PC; such attempts have included dynamic studies and MR spectroscopy, which provided promising but inconsistent results (6–16). Diffusion-weighted images (DWI) and calculated apparent diffusion coefficient (ADC) mapping are additional approaches, involving the representation of the Brownian movement of water molecules. This new parameter dif-

[1]Department of Clinical Radiology, Graduate School of Clinical Sciences, Kyushu University, Fukuoka, Japan.
[2]Department of Anatomic Pathology, Graduate School of Clinical Sciences, Kyushu University, Fukuoka, Japan.
[3]Department of Urology, Graduate School of Clinical Sciences, Kyushu University, Fukuoka, Japan.
*Address reprint requests to: K.Y., Department of Clinical Radiology, Graduate School of Medical Sciences, Kyushu University, 3-1-1, Maidashi, Higashi-ku, Fukuoka, 812-8582, Japan.
E-mail kengo@med.kyushu-u.ac.jp
Received December 31, 2006; Accepted August 29, 2007.
DOI 10.1002/jmri.21181
Published online in Wiley InterScience (www.interscience.wiley.com).

fers from conventional T1 or T2 relaxivity, dynamic enhancement characteristics, or spectroscopic information. This DWI or the ADC map has been applied for examining various part of the body, in particular to detect or differentiate malignancies (17–20). Regarding PC, several preliminary investigations have been sporadically reported (21–25), with promising results. In this article, we applied the ADC map obtained from DWI to the diagnosis of PC, and evaluated its performance at detecting and localizing PC using stepwise histopathological data as a gold standard. We also correlated the results to the histological grades of the lesions and Gleason's scores (GS) of the specimens, in order to characterize the potential clinical usefulness of this novel technique.

MATERIALS AND METHODS

Patients

Between January 2000 and March 2004, 124 patients underwent radical prostatectomy at our institute. Among these patients, 37 who had undergone preoperative MRI (including DW imaging) were retrospectively selected, and these 37 patients formed the present study population. One of the 37 subjects had received hormonal therapy prior to surgery. The age of the selected patients ranged from 56 to 75 years old (mean = 66 years). The preoperative prostate-specific antigen (PSA) level ranged from 0.7 to 54.8 ng/mL, with a mean of 11.9 (normal range < 4.00 ng/mL). All subjects had undergone transrectal or transperineal biopsy prior to MR imaging and had been pathologically diagnosed with malignant foci in the prostate. The period between biopsy and MR ranged from six to nine weeks (mean = 7.2 weeks), and the period between MR and surgery ranged from zero to eight weeks (mean = 2.5 weeks). The institutional review board at our hospital did not require that written informed consent be obtained for this study due to its retrospective nature. The current study was designed and performed according to the declaration of Helsinki (26).

MR Equipment and Parameters

A total of two 1.5T units (Magnetom Symphony and Vision; Siemens, Erlangen, Germany) were used with a pelvic multichannel phased-array coil (12 channels). After routine T1-weighted spin-echo (TR/TE/number of excitations [NEX] = 500 msec/12 msec/2) axial images had been obtained, T2-weighted fast spin-echo (TR/TE/Turbo factor/NEX = 3000 msec/102 msec/15/3, slice thickness = 5 mm, interslice gap = 30%) axial and coronal images with axial DWI were obtained using the single-shot spin-echo echo-planar imaging (EPI) technique. The matrix and field-of-view of the T1- and T2-weighted images (T1WI and T2WI) were 256 × 512, and 20 cm, respectively. The slice thickness and gap of DWI were identical to those of routine T1WI and T2WI. Sequential sampling of the k-space was used with echo-time (TE) = 110–135 msec and bandwidth = 1250 Hz/pixel, and 128 lines of data were acquired in 0.3 seconds. No parallel imaging technique was applied. Other parameters included a field-of-view = 240 mm, matrix size = 128 × 128, and the acquisition of four signals. All images were obtained while the patients maintained normal and consistent breathing, and a fat-saturated pulse was used for the DWI to exclude severe chemical-shift artifacts. A contrast-enhanced dynamic study was performed and postcontrast T1WI were obtained in all cases, the details of which are not given here, as they are out of the scope of this work.

DWI were acquired with motion-probing gradient pulses applied along three (x-, y-, and z-axes) directions with three b factors of 0, 500, and 1000 seconds/mm^2. ADC maps were automatically generated on the operating console using all seven images (b = 0 and two b-values in each direction), and the ADC values were obtained by measuring the intensity of the map.

Pathological Map Preparation

One experienced pathologist created transverse sections of the specimens: the most apical and basic sides of the specimen were cut to a thickness of 6 mm, and the remaining portion (majority of the specimen) were cut to a thickness of 4 mm. Each section of each specimen was digitally photographed together with a ruler along the edge, which serve as a size reference, and the areas of the PC that had been microscopically determined were marked on the digital photographs by the pathologist (pathological map) using commercially available presentation software (Microsoft PowerPoint 2002; Microsoft Corporation, Redmond, WA, USA). All PC foci, including infiltrating foci that did not form apparent masses, were marked on the map and divided into the sextants according to their location, as follows: right and left apices (lower third), midglands (middle third), and bases (upper third). Lesions consisting of uniform histological grades were also documented as such on the photograph. This pathological map was used as the gold standard in this study.

Assessment

First, we subdivided the glands of all patients into sextants on the MR images. The presence of PC in each sextant was retrospectively evaluated and recorded by two radiologists in a consensus. Initially, T2WI alone (T2WI reading) were interpreted and then T2WI and the ADC map (T2WI/ADC map reading) were interpreted. The readers were informed that the patients had undergone surgery for PC, but no other clinical information, (e.g., PSA level or biopsy results) was provided to the readers. On either T2WI or the ADC map, areas with apparently lower signal intensity than that of the surrounding tissue were considered to represent PC, according to the previously reported descriptions (5–16,21–25). Regarding T2WI/ADC map reading, when the findings on either sequence were equivocal, those on the ADC map were considered to have priority, if image degradation is not prominent. Sensitivity and specificity were thus calculated based on the sextant evaluation and the results of the two interpretations were compared.

We then directly compared the MR images and the pathological map on a lesion basis, and we excluded

positive sextants in which the noncancerous areas had been interpreted as PC on the MR images (false-positive lesions in positive sextants); thus the true sensitivity was calculated. As for a lesion whose location at least partially overlapped on the MR images and on the pathological map, the lesion was considered false-positive when the maximum transverse diameter measured at MRI was out of the range of 50% to 150% of the maximum transverse diameter measured on the pathological map (16). Lesions seen at MRI were only considered truly positive if the suspected foci were in the same relative portion of the prostate.

We also marked the approximate areas of PC on a pathological map, which had been detected on MR images (detected PC) using MR images as reference, and the areas of the whole PC and the detected PC were traced and measured using NIH software (NIH Image, version 1.63; National Institutes of Health, Bethesda, MD, USA). Volume was calculated by multiplying the measured areas by thickness (0.4 cm). False-positive lesions, including those in positive sextants as defined above, were excluded in this evaluation. Thus, % tumor volume (percentage of the tumor volume detected to the whole tumor volume; range = 0–100%) per patient was compared between the T2WI reading and T2WI/ADC map reading. The lesions were subclassified into peripheral zone (PZ) and transitional zone (TZ) lesions according to their location on the pathological map, and these two groups were compared in terms of % tumor volume per patient. Then, the % tumor volume per patient was also correlated to the GS of the patients.

Lesions with uniform histological grades that were larger than 1 cm in their short axes were selected on the pathological map and their ADC values were measured at the corresponding sites on the ADC map by one radiologist, even when there were no detectable abnormal areas on the ADC map. Correlation of ADC value and histological grades was thus evaluated. We also evaluated the detectability of these lesions in correlation with the their histological grades.

Finally, by comparing the MR images and pathological maps, we selected areas of PC larger than 1 cm in their short axes that had not been detected on ADC map (false-negative lesions). The possible reasons for these lesions not being detected on MR images were analyzed. We also selected areas of low signal intensity larger than 1 cm in their short axes on the ADC map that did not correspond to PC on the pathological map (false-positive lesions). The corresponding sites were marked on the pathological map, and pathological details of these areas were then reevaluated by the pathologist.

RESULTS

In one patient, microscopic evaluation of the resected gland revealed no PC, although preoperative biopsy had suggested the presence of PC in one of the sextants. A total of 222 sextants in 37 patients were evaluated, among which 147 sextants were positive and 75 were negative for the presence of PC. A total of 79 and 105 positive sextants, and 45 and 46 negative sextants were correctly diagnosed with T2WI reading and T2WI/ADC map reading, respectively. Among the 79 and 105 positive sextants that were classified as positive, 45 and 31 were excluded for the calculation of true sensitivity because they were regarded as noncancerous areas on the lesion-based evaluation. The sensitivity, true sensitivity, and specificity of T2WI reading were 53%, 23%, and 60%, whereas the sensitivity, true sensitivity, and specificity of the T2WI/ADC map reading were 71%, 50%, and 61%, respectively. There was a significant difference between the two interpretations in terms of the sensitivity and true sensitivity ($P < 0.01$, McNemar chi-squared test), but no difference in the specificity ($P = 0.97$).

The areas of PC on the pathological map ranged from 3 mm to 22 mm in their shortest dimension (mean = 7 mm). The calculated volumes of PC per patient ranged from 0 to 5.75 cm^3 (mean = 1.49 cm^3). There were 261 and 151 areas of the PC in PZ and TZ; the sum of tumor volume were 38.8 and 16.3 cm^3, respectively. The majority (33/37) of our patients had areas of PC in both PZ and TZ. The mean % tumor volume per patient detected by T2WI reading were 20% (range = 0–100%), 41% (range = 0–100%), and 7% (range = 0–91%), for total lesions, the PZ lesions, and TZ lesions, respectively. The mean % tumor volume per patient detected by T2WI/ADC map reading for total lesions, the PZ lesions, and TZ lesions, were 47% (range = 0–100%), 48% (range = 0–100%), and 44% (range = 0–100%), respectively. Overall (not per patient, but total sum) % tumor volume by T2WI reading were 30%, 55%, and 20%, for total lesions, the PZ lesions, and TZ lesions, respectively. Overall % tumor volume by T2WI/ADC map for total lesions, the PZ lesions, and TZ lesions, reading were 55%, 57%, and 52%, respectively. Addition of the ADC map to T2WI interpretation revealed a significant increase in % tumor volume in total lesions ($P = 0.0002$, Wilcoxon signed rank test) and in TZ lesions ($P < 0.0001$), but not in PZ lesions ($P = 0.158$, not significant [NS]).

For the resected specimens in 35 patients (excluding one patient whose specimen revealed no evidence of PC and another who had received hormonal therapy), GS were assigned. There was a weak but significant correlation between % tumor volume by T2WI/ADC map reading and GS ($\rho = 0.40$, $P = 0.022$, Spearman's rank correlation test) (Fig. 1). Patients with higher GS tended to have higher % tumor volume, namely had more chance for PC to be detected by T2WI/ADC map reading. No significant correlation was observed between % tumor volume detected by T2WI reading alone and GS ($P = 0.41$, NS). Because it has been reported that the larger the tumor is, there is the better correlation between tumor volume measured on T2WI and histopathologic volume (14), we might need to exclude the effect of the volume of PC in evaluating the correlation between % tumor volume by T2WI/ADC map reading and GS. We therefore evaluated the partial correlation coefficient between either tumor volume or GS and % tumor volume detected (Table 1). The results showed that % tumor volume detected with T2WI/ADC map reading significantly correlated to GS, but not to tumor volume, and also that % tumor volume detected with T2WI reading correlated to the tumor volume, but not to GS.

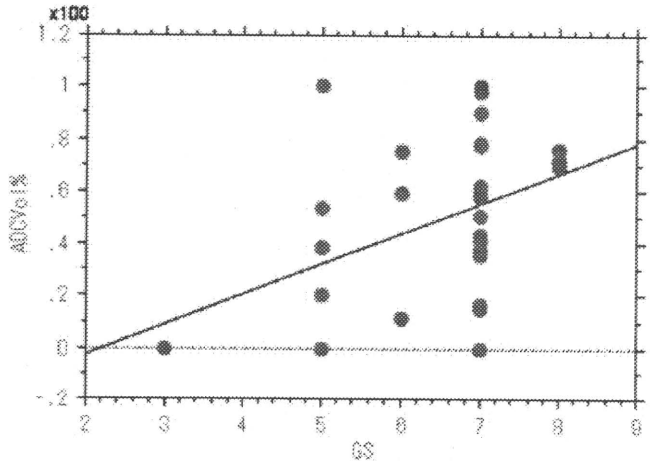

Figure 1. Correlation between % tumor volume detected by T2WI and ADC map interpretation and GS of the specimens. There was a weak but significant correlation (ρ = 0.40, P = 0.022, Spearman's rank correlation test). ADC Vol% = % tumor volume detected with T2WI and ADC map interpretation, GS = Gleason's scores.

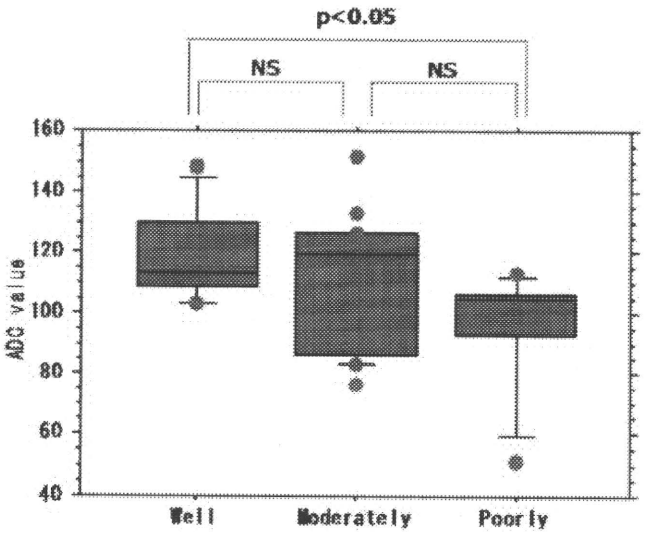

Figure 2. Correlation between ADC values and histological grades of PC. ADC values of well-, moderately-, and poorly-differentiated adenocarcinoma were 1.19 ± 0.15, 1.10 ± 0.24, and 0.93 ± 0.20 × 10^{-3} mm^2/second (mean ± SD), respectively. Difference was significant only between well- and poorly-differentiated carcinoma (P = 0.019, one-way factorial ANOVA with Scheffe's post-hoc test). There was a subtle, but significant correlation (Spearman's rank correlation test, ρ = −0.144, P = 0.045). A horizontal line in the middle of each box indicates a median of each group. [Color figure can be viewed in the online issue, which is available at www.interscience.wiley.com.]

Regarding the ADC value measurement, 53 lesions with uniform histological grades that were larger than 1 cm in their short axes were selected from 36 patients. There were 21, 26, and six lesions, in well-, moderately-, and poorly-differentiated adenocarcinomas, respectively. The mean size (short axis diameter) of these lesions was 1.14 cm (range: 1.0–1.9 cm), 1.23 cm (1.0–2.2 cm), and 1.03 cm (1.0–1.2), respectively, showing no significant difference (P = 0.38, one-way factorial analysis of variance [ANOVA]). The ADC values of well-, moderately-, and poorly-differentiated PC were 1.19 ± 0.15, 1.10 ± 0.24, and 0.93 ± 0.20 × 10^{-3} mm^2/second (mean ± standard deviation [SD]), respectively. Significant difference in ADC values was seen only between well- and poorly-differentiated PC (P = 0.019), and difference between well- and moderately-differentiated, or that between moderately- and poorly-differentiated PC was not significant (P = 0.38 and 0.13, one-way factorial ANOVA with Scheffe's post hoc test). There was a subtle but significant correlation between the histological grades and ADC values (ρ = −0.18, P = 0.014, Spearman's rank correlation) (Fig. 2). Of these 53 lesions, 13 (62%), 24 (92%), and six (100%) were detected on the ADC map, in well-, moderately-, and poorly-differentiated adenocarcinomas, respectively. The detectability of these lesions differed significantly among histological grades (Kruskal-Wallis test, P < 0.01) and a significant correlation was observed, whereby the less differentiated lesions were associated with higher detectability (P < 0.01, Cochran-Armitage test for trend).

Table 1
Partial Correlation Coefficient Based on Spearman's Rank Correlation Coefficient Between Either Tumor Volume or Gleason's Score and % Tumor Volume Detected by T2WI Reading Alone and T2WI/ADC Map Reading

	% Tumor volume detected	
	T2WI	T2WI/ADC map
Tumor volume		
Partial ρ	0.4439	0.045
P-value	0.0109	0.8065
Gleason's score		
Partial ρ	−0.0535	0.3507
P-value	0.7712	0.0491

T2WI = T2-weighted image reading, T2WI/ADC map = T2-weighted image and apparent diffusion coefficient map reading, ρ = correlation coefficient.

As for false-positive lesions, 54 foci were selected from 27 patients. The pathological details of these lesions included hyperplastic nodules in 22, normal structure in 14 (periejaculatory duct tissue in five, asymmetric central zone tissue in four, base of the seminal vesicle in three, asymmetric anterior fibromuscular stroma in one, and vermontanum in one), intraacinar hemorrhage in 10, and chronic prostatitis in eight. As for false-negative lesions, 15 foci in 15 patients were selected. Possible causes for these false-negatives were well-differentiated infiltrative lesions with preserved gland formation in six lesions, susceptibility artifact from rectal or intestinal gas in four lesions, and susceptibility artifact from metallic prosthesis at the hip joint in one lesion. Causes for the remaining four lesions remained unknown. Representative cases are shown in Figs. 3, 4, and 5.

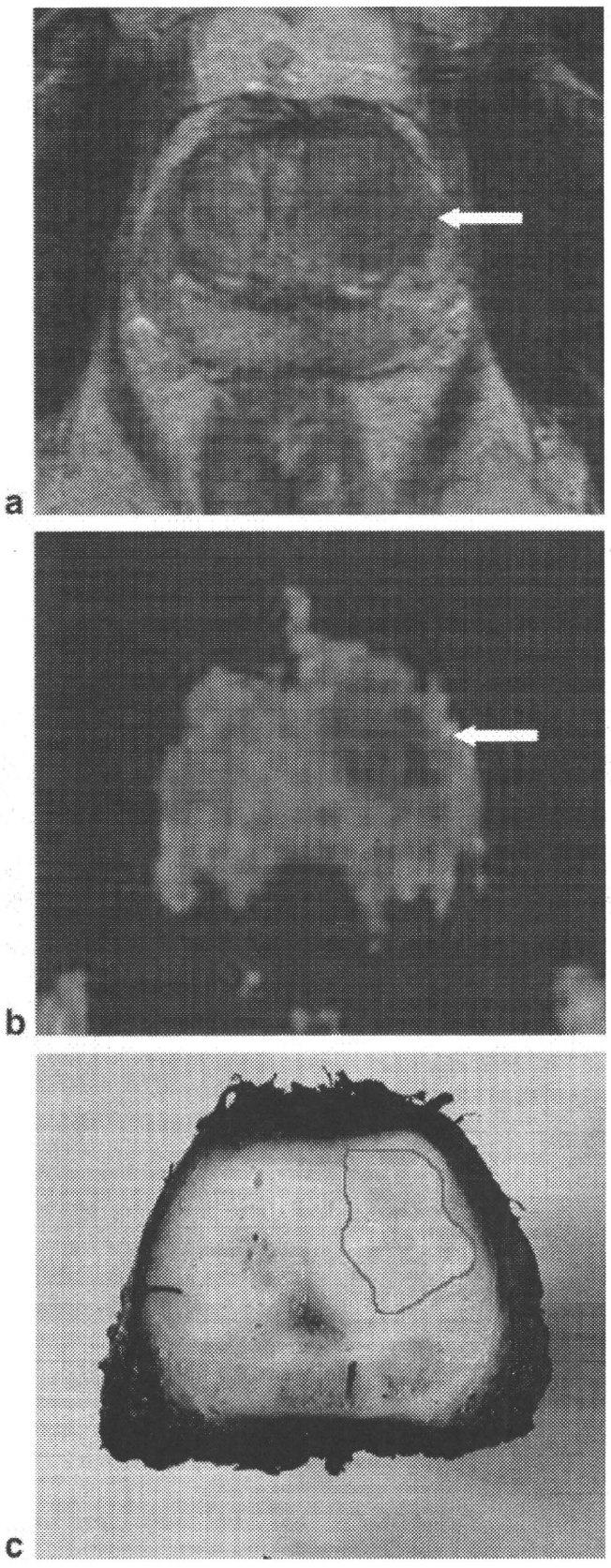

Figure 3. A 69-year-old man with a preoperative PSA level of 12.5 ng/mL. There was a moderately differentiated adenocarcinoma at the left TZ (GS: 3 + 5 = 8) confined within the gland. Both T2WI (**a**) and ADC map (**b**) clearly demonstrated carcinoma as low signal intensity areas (arrows). An encircled area represents the carcinoma on the pathological map (**c**). [Color figure can be viewed in the online issue, which is available at www.interscience.wiley.com.]

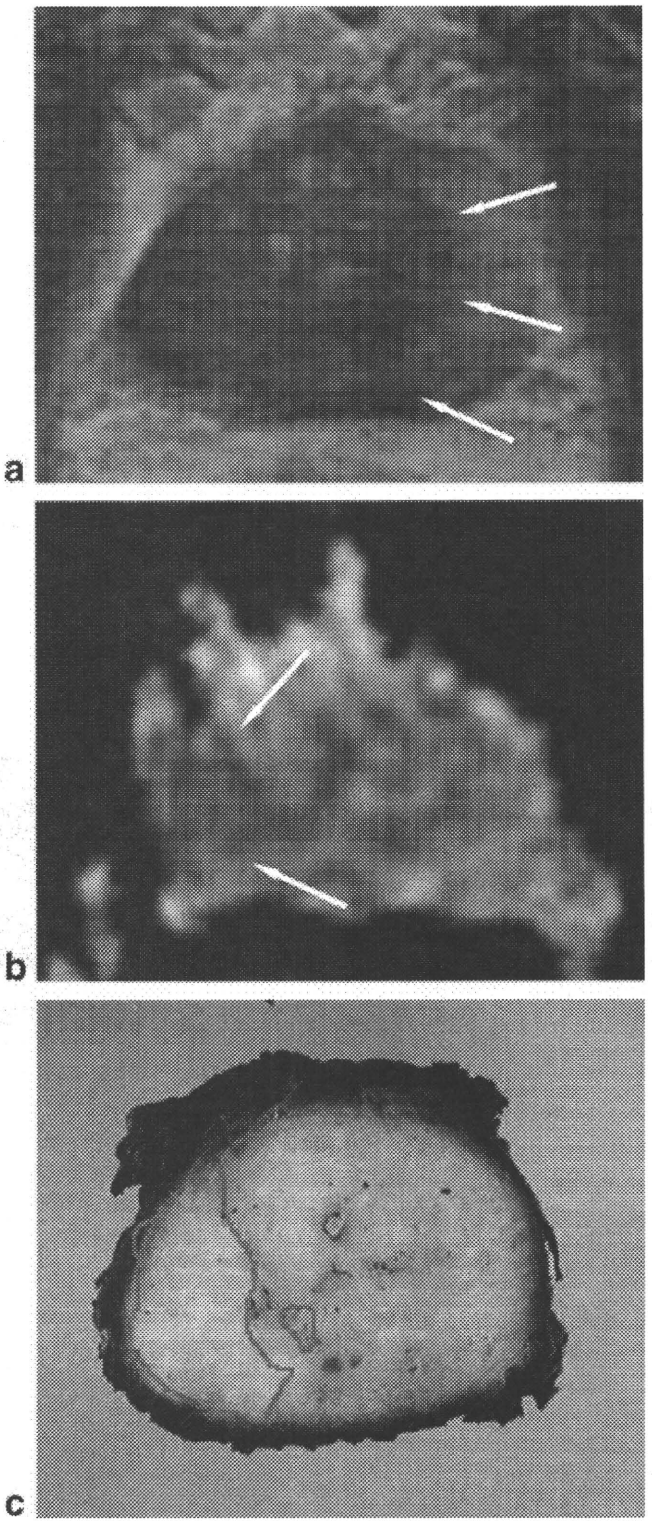

Figure 4. A 63-year-old male with an initial PSA level of 16 ng/mL. The patient received hormonal therapy using chrormadinone acetate and leuprorelin acetate for three months and the PSA level decreased to 0.8 ng/mL just before surgery. There was a moderately- to poorly-differentiated adenocarcinoma at the right PZ, confined within the gland. GS was not evaluated because of cellular degeneration. On T2WI (**a**), approximately two-thirds of the gland on the right exhibited low signal intensity (arrows). On ADC map (**b**), an area of low signal was localized at the right PZ (arrows), which corresponded well to the area of carcinoma shown on the pathological map (**c**) (encircled areas). [Color figure can be viewed in the online issue, which is available at www.interscience.wiley.com.]

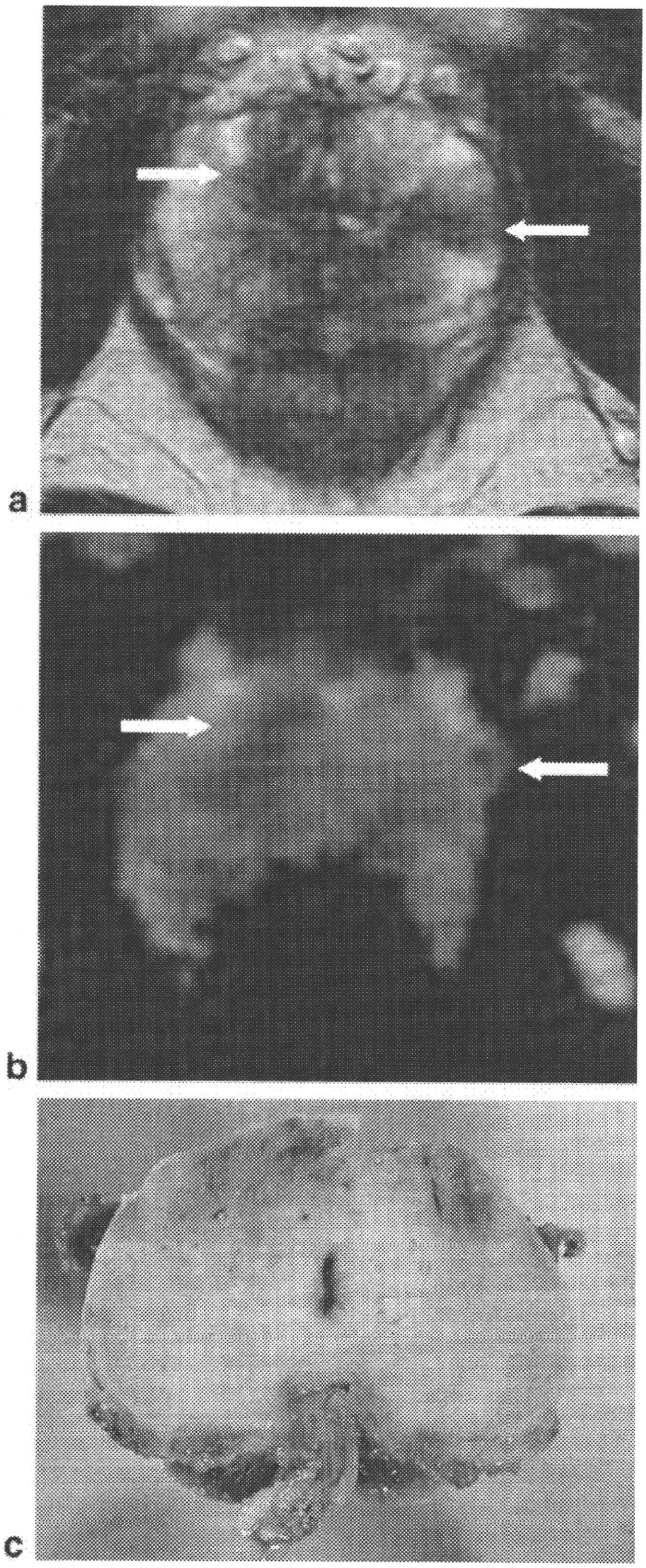

Figure 5. A 59-year-old male with a preoperative PSA level of 0.7 ng/mL and positive biopsy results. There was a small focus (3 mm in diameter) of well-differentiated adenocarcinoma at the apex of the gland (not shown), with a GS of 3 + 2 = 5. The major portion of the gland was free of carcinoma cells. There were several areas of low signal intensity, both on T2WI (**a**) and ADC map (**b**) (arrows); however, there was no carcinoma at the corresponding sites on the pathological map (**c**). Hyperplastic glandular and interstitial cells were noted at theses sites upon reevaluation of the specimen. [Color figure can be viewed in the online issue, which is available at www.interscience.wiley.com.]

DISCUSSION

Previous investigators have reported significant difference in ADC values between PC and normal prostatic tissue, using biopsy-proven histopathology as a reference (21–25). To date, there have been few reports regarding PC detection with DWI or ADC mapping in patients who had undergone prostatectomy. We therefore attempted in the present study to clarify the clinical usefulness and significance of DWI or ADC mapping using a stepwise histopathology as a gold standard.

According to our results, sextant-based sensitivity and true sensitivity improved significantly, i.e., up to 71% and 50%, respectively, when the ADC map was interpreted along with T2WI, although the specificity remained unchanged at around 60%. In terms of the volume of PC, T2WI/ADC map reading detected approximately one-half of the tumor in the gland. Previously reported sensitivity and/or detection rate of PC on MRI (i.e., T2WI with or without spectroscopy), has been in a range between 20% to 80% (6–16). Recently, Hom et al (16) reported a detection rate of around 20% using endorectal coil MR images and MR spectroscopy for cases of PC in PZ, and using meticulous histopathologic evaluation methods and strict criteria. Our data also revealed a rather low sensitivity or detection rate, at least in part because we also used the pathological map as a strict gold standard, including all small foci of PC. Another explanation for this low sensitivity may have been the criteria we used to detect PC in our study. Namely, we considered "areas with low signal intensity relative to the surrounding tissue" as PC in both PZ and TZ; however, Li et al (27) recently applied more meticulous criteria to diagnose TZ lesions and achieved better results. Although the application of different criteria might have improved the sensitivity, our present data suggest that a T2WI/ADC map reading cannot be used as a reasonable guide yet in localization of PC in the context of local therapies such as IMRT or HIFU. Practical use of ADC maps may therefore be limited at present, for example, to a guide for rebiopsy in patients with high PSA levels but with negative biopsy results.

To improve sensitivity of the T2WI/ADC map reading, it will be necessary to detect well-differentiated PC with glandular formation, which was the most common cause of false negativity in our series. In our evaluation of the lesions larger than 1 cm in the shortest dimension, the ADC values of well-differentiated PC were significantly higher than moderately- or poorly-differentiated PC, and nearly one-half of these lesions were visually missed on the T2WI/ADC map interpretation. The pathological architecture of these lesions, namely, preserved glandular formation with a significant volume of fluid-filled luminal space, which is similar to that of normal prostatic glandular tissue, supports the relatively high ADC values of these lesions; these features rendered it difficult to detect such lesions on the ADC map. Improving the signal-to-noise ratio (SNR) by using 3T hardware or a coil with more channels may help detect these lesions. Concurrent usage of a parallel imaging technique (24,28,29) may also help reduce the susceptibility artifacts, the second most common cause of false negativity.

To improve specificity, it will be necessary to differentiate between hyperplastic nodules and PC; the lack of such differentiation was the most common cause of false positivity in our results. Again, improving the SNR by either the use of 3T hardware or new coils may help differentiate these two entities. The second most common reason for false positivity was normal prostatic tissue, including periejaculatory duct tissue, central zone tissue, tissue at the base of the seminal vesicle, and so on. The ADC values of these structures were $0.97 \pm 0.18 \times 10^{-3}$ mm^2/second (not shown in the results), which were within the range of ADC values of PC. Precise anatomic evaluation may obviate this misdiagnosis; however, it would remain difficult to discriminate these structures from focal involvement of PC on an ADC map. Combination with MR spectroscopy or dynamic MR study may be of some help in resolving this problem.

The promising aspects of our findings are as follows. First, the T2WI/ADC map reading significantly increased the detection of PC located in TZ. In terms of the % tumor volume, the detection rate of T2WI/ADC map reading was approximately 50% regardless of the location of PC, whereas that of T2WI reading alone was significantly worse in the case of lesions in TZ than in those in PZ. Because PC in TZ has remained a diagnostic problem either for transrectal ultrasound (US) or conventional MR, use of DWI and ADC maps could be of aid in the detection of lesions in TZ in particular. Although Li et al (27) recently reported improved detection of PC in TZ using the combined criteria of T2WI and postcontrast T1WI, adding information of ADC map might further improve the detection of PC in TZ.

A second promising point suggested by our results was that the higher the histological grade of PC, the lower the ADC values of PC, which increases the chances of PC being detected on an ADC map. This finding may also be related to the positive correlation between % tumor volume detected by T2WI/ADC map reading and GS (Table 1). Such information may be clinically important because it may suggest that the biologically aggressive components or subsets of PC are more likely to be detected by T2WI/ADC map reading than would less aggressive components. As the histological grade or GS increases, there have been shown to be more chances of cellular architectures exhibiting little gland formation, such as medullary or solid patterns (30,31); these features may explain the low ADC values in these lesions. Although the ADC values obtained in our study were comparable to the previously reported values (21–25), this is the first study to reveal the relationship between histological grade or GS and ADC values in cases of PC.

A third promising issue suggested by the results from but a single patient was that the areas of PC was relatively clearly depicted on ADC map within areas of diffusely decreased signal intensity on T2WI; this was a patient who had received preoperative hormonal therapy (androgen deprivation) (Fig. 4). It was already well known that posthormonotherapy prostatic tissue becomes atrophic and diffusely hypointense, which impairs pertinent MR detection of PC (32,33). The ADC map might be of help in evaluating patients still undergoing or following hormonal therapy.

There are several limitations to the present study. First, this study was retrospective in nature, and all patients in this series had undergone biopsy prior to MR examination. Although the period between biopsy and MR examination in our study was more than one month, which is reportedly sufficient to avoid biopsy effects on MR images (34,35), the histopathological evaluation revealed intraacinar hemorrhage, which was the third most common cause of false positivity. Another technical aspect related to the retrospective nature of the study was the subtle differences between MR images and pathological section in terms of the slice interval and slice direction; such differences might have exerted an influence on the precise correlation between the depicted abnormality and the lesions observed on the pathological map. Prospective studies are needed that are designed in such a manner that MR examination is performed prior to biopsy and in which the MR and pathological sections are identical. In addition, due to the limitation associated with the hardware, TE of EPI used for the DWI was rather long (110–135 msec) in our study, as compared to that of previous reports (96–120 msec) (21–25). This long TE may have led to the low SNR of the images, particularly in cases involving tissues with short T2 characteristics, which in turn possibly led to the incorrect calculation of ADC values. Use of a parallel imaging technique might have improved this situation, allowing for a shorter TE (24,28,29), although this technique was not available at the time we started this study. Third, because of the significant image distortion of the ADC map, we did not perform any volume measurement on MR images, although in this study, such measurements were carried out on the pathological map by encircling the approximate area of PC by visual inspection using MR images as a reference. Again, a parallel imaging technique would have been useful to reduce the image distortion secondary to the susceptibility effect from intestinal gas or metallic prosthesis (24,28,29), which would in turn have enabled us to measure the areas of interest on the ADC map.

In conclusion, the ADC map derived from DWI of MRI performed with a phased array coil without parallel imaging technique significantly improved PC detection and localization when interpreted together with T2WI, although the performance of this method might not yet be sufficient for it to serve as a guide for local therapies. This novel approach to the diagnosis of PC is expected to be particularly useful for the detection of PC lesions located in TZ, as well as detection of lesions with relatively little differentiation, and lesions with a relatively high GS.

ACKNOWLEDGMENT

We thank Professor Masasumi Tsuneyoshi, Chair of the Department of Anatomic Pathology, Graduate School of Medical Sciences, Kyushu University, for providing us pathologic specimens for this study.

REFERENCES

1. American Cancer Society. Cancer Facts and Figures 2004. Atlanta, GA: American Cancer Society; 2004. 60 p. Available at: http://www.cancer.org/downloads/STT/CAFF_finalPWSecured.pdf. Last accessed: September 20, 2007.
2. Carroll PR, Presti JC Jr, Small E, Roach M III. Focal therapy for prostate cancer 1996: maximizing outcome. Urology 1997; 49(Suppl 3A):84–94.
3. Meerleer GD, Villeirs G, Bral S, et al. The magnetic resonance detected intraprostatic lesions in prostate cancer: planning and delivery of intensity-modulated radiotherapy. Radiother Oncol 2005;75:325–333.
4. Blana A, Walter B, Rogenhoer S, Wieland W. High-intensity focused ultrasound for the treatment of localized prostate cancer: 5-year experience. Urology 2004;63:297–300.
5. Rajesh A, Coakley FV. MR imaging and MR spectroscopic imaging of prostate cancer. Magn Reson Imaging Clin N Am 2004;12:557–579.
6. Engelbrecht MR, Huisman HJ, Laheij RJ, et al. Discrimination of prostate cancer from normal peripheral zone and central gland tissue by using dynamic contrast-enhanced MR imaging. Radiology 2003;229:248–254.
7. Hasumi M, Suzuki K, Taketomi A, et al. The combination of multivoxel MR spectroscopy with MR imaging improve the diagnostic accuracy for localization of prostate cancer. Anticancer Res 2003; 23:4223–4227.
8. Ikonen S, Kivisaari L, Tervahartiala P, Vehmas T, Taari K, Rannikko S. Prostatic MR imaging. Accuracy in differentiating cancer from other prostatic disorders. Acta Radiol 2001;42:348–354.
9. Dhingsa R, Qayyum A, Coakley FV, et al. Prostate cancer localization with endorectal MR imaging and MR spectroscopic imaging: effect of clinical data on reader accuracy. Radiology 2004;230:215–220.
10. Kurhanewicz J, Swanson MG, Nelson SJ, Vigneron DB. Combined magnetic resonance imaging and spectroscopic imaging approach to molecular imaging of prostate cancer. J Magn Reson Imaging 2002;16:451–463.
11. Kumar R, Kumar M, Jagannathan NR, Gupta NP, Hemal AK. Proton magnetic resonance spectroscopy with a body coil in the diagnosis of carcinoma prostate. Urol Res 2004;32:36–40.
12. Kiessling F, Huber PE, Grobholz R, et al. Dynamic magnetic resonance tomography and proton magnetic resonance spectroscopy of prostate cancers in rats treated by radiotherapy. Invest Radiol 2004;39:34–44.
13. Kaji Y, Wada A, Imaoka I, et al. Proton two-dimensional chemical shift imaging for evaluation of prostate cancer: external surface coil vs. endorectal surface coil. J Magn Reson Imaging 2002;16:697–706.
14. Coakley FV, Kurhanewicz J, Lu Y, et al. Prostate cancer tumor volume: measurement with endorectal MR and MR spectroscopic imaging. Radiology 2002;223:91–97.
15. Purohit RS, Shinohara K, Meng MV, Carroll PR. Imaging clinically localized prostate cancer. Urol Clin North Am 2003;30:279–293.
16. Hom JF, Coakley FV, Simko JP, et al. Prostate cancer: endorectal MR imaging and MR spectroscopic imaging—distinction of true-positive from chance-detected lesions. Radiology 2006;238:192–199.
17. Ichikawa T, Haradome H, Hachiya J, Nitatori T, Araki T. Diffusion-weighted MR imaging with a single-shot echoplanar sequence: detection and characterization of focal hepatic lesions. AJR Am J Roentgenol 1998;170:397–402.
18. Castillo M, Smith JK, Kwock L, Wilber K. Apparent diffusion coefficients in the evaluation of high-grade cerebral gliomas. AJNR Am J Neuroradiol 2001;22:60–64.
19. Nakayama T, Yoshimitsu K, Irie H, et al. Usefulness of the calculated apparent diffusion coefficient value in the differential diagnosis of retroperitoneal masses. J Magn Reson Imaging 2004;20:735–742.
20. Nakayama T, Yoshimitsu K, Irie H, et al. Diffusion-weighted echoplanar MR imaging and ADC mapping in the differential diagnosis of ovarian cystic masses: usefulness of detecting keratinoid substances in mature cystic teratomas. J Magn Reson Imaging 2005; 22:271–278.
21. Gibbs P, Tozer DJ, Liney GP, Turnbull LW. Comparison of quantitative T2 mapping and diffusion-weighted imaging in the normal and pathologic prostate. Magn Reson Med 2001;46:1054–1058.
22. Issa B. In vivo measurement of the apparent diffusion coefficient in normal and malignant prostatic tissues using echo-planar imaging. J Magn Reson Imaging 2002;16:196–200.
23. Hosseinzadeh K, Schwarz SD. Endorectal diffusion-weighted imaging in prostate cancer to differentiate malignant and benign peripheral zone tissue. J Magn Reson Imaging 2004;20:654–661.
24. Sato C, Naganawa S, Nakamura T, et al. Differentiation of noncancerous tissue and cancer lesions by apparent diffusion coefficient values in transition and peripheral zones of the prostate. J Magn Reson Imaging 2005;21:258–262.
25. Shimousa R, Fujimoto H, Akamata H, et al. Diffusion-weighted imaging of prostate cancer. J Comput Assist Tomogr 2005;29:149–153.
26. World Medical Association. Declaration of Helsinki: ethical principles for medical research involving human subjects. Ferney-Voltaire, France: World Medical Association; 2004. 5p. Available at: http://www.wma.net/e/policy/b3.htm. Last accessed: September 20, 2007.
27. Li H, Sugimura K, Kaji Y, et al. Conventional MR capabilities in the diagnosis of prostate cancer in the transition zone. AJR Am J Roentgenol 2006;186:729–742.
28. Sodickson DK, McKenzie CA. A generalized approach to parallel magnetic resonance imaging. Med Phys 2001;28:1629–1643.
29. Jaermann T, Crelier G, Pruessmann KP, et al. SENSE-DTI at 3 T. Magn Reson Med 2004;51:230–236.
30. Gleason DF, Vacu RG. Histologic grading and clinical staging of prostatic carcinoma. In: Tannenbaum M, editor. Urologic pathology: the prostate. Philadelphia: Lea and Febiger; 1997. p 171–197.
31. Epstein JI. Urinary tract and male genital system. The prostate and seminal vesicle. In: Sternberg SS, editor. Diagnostic surgical pathology. New York: Raven Press; 1989. p 1393–1432.
32. Chen M, Hricak H, Kalbhen CL, et al. Hormonal ablation of prostatic cancer: effects on prostate morphology, tumor detection, and staging by endorectal coil MR imaging. AJR Am J Roentgenol 1996; 166:1157–1163.
33. Padhani AR, MacVicar AD, Gapinsli CJ, et al. Effects of androgen deprivation on prostatic morphology and vascular permeability evaluated with MR imaging. Radiology 2001;218:365–374.
34. White S, Hricak H, Forstner R, et al. Prostate cancer: effect of post-biopsy hemorrhage on interpretation of MR images. Radiology 1995;195:385–390.
35. Ikonen S, Kivisaari L, Vehmas T, et al. Optimal timing of post-biopsy MR imaging of the prostate. Acta Radiol 2001;42:70–73.

Fate of Seminal Vesicles and Prostate After Medical Castration: How Long Is the Optimal Duration of Neoadjuvant Treatment for Prostate Cancer Before Radiation?

Ryoji Furuya, Shin-ichi Hisasue, Seiji Furuya, Nobuhito Saitoh, Hiroshi Ogura, Satoshi Takahashi, and Taiji Tsukamoto

OBJECTIVES To clarify the morphological alteration of prostate and seminal vesicles (SV) quantitatively after testosterone ablation, we investigated the prostate volume (PV) and the SV volume (SVV) using transrectal ultrasonography.

METHODS Between July 2002 and October 2004, we prospectively investigated 29 prostate cancer patients. The medical castration group included 21 patients (42 SV and 21 prostate; median Gleason sum, 74 years) who were diagnosed as having T1b to T3aN0M0 prostate cancer and underwent androgen ablation with a luteinizing hormone-releasing hormone (LH-RH) analogue and chlormadinone acetate. As normal controls, 8 patients (16 SV and 8 prostate; median age, 68.5 years) with T1aN0M0 prostate cancer without any other additional treatment were enrolled in this study. We measured both PV and SVV in these groups with transrectal ultrasonography.

RESULTS Both PV and SVV significantly decreased in the medical castration group (PV: 28.4 ± 9.3 mL to 17.0 ± 5.3 mL, SVV: 3.5 ± 1.8 mL to 1.9 ± 1.0 mL; median, 6 months), whereas those in the control group were maintained (PV: 16.6 ± 5.7 mL to 16.5 ± 5.3 mL, SVV: 2.5 ± 1.0 mL to 2.6 ± 1.6 mL; median, 12 months). In longitudinal assessment, mean PSA, PV, and SVV were significantly reduced gradually up to 12 months after medical castration.

CONCLUSIONS Not only PV but also SVV was significantly reduced after medical castration. Moreover, size reduction continued up to 12 months in SV, with especially marked reduction seen through the first 6 months. These results demonstrated that optimum duration for androgen ablation before radiotherapy is at least 6 months, and up to 12 months for the maximum effect. UROLOGY 72: 417–421, 2008. © 2008 Elsevier Inc.

It has been established that the size of male reproductive organs such as the testis, seminal vesicles (SV), and prostate depends on the androgen level, which was quantitatively analyzed in animal models.[1–4] However, there are few reports regarding such an analysis for humans.[5] Furthermore, to our knowledge, there has been no report on either longitudinal or quantitative analysis regarding volume reduction of the human prostate and SV after androgen ablation.

Radiotherapy is known to be highly effective for organ-confined or locally advanced prostate cancer.[6,7] However, it has also been suggested that for some cases radiotherapy alone is not sufficient.[8] Volume reduction of the prostate and SV has a considerable effect on the treatment strategy to enhance the efficacy and the safety of radiotherapy for T2 or T3 prostate cancer.[9] It has not been established, however, how long patients should undergo hormonal treatment before radiation from the aspect of the morphological changes of the prostate and SV. Thus, to optimize the radiotherapy strategy for prostate cancer, we investigated the morphological alterations of both SV volume (SVV) and prostate volume (PV) quantitatively after medical castration.

MATERIAL AND METHODS

Between July 2002 and October 2004, 29 prostate cancer patients were enrolled and investigated prospectively. The medical castration group included 21 patients (42 SV and 21 prostate), who were diagnosed as having T1b to T3aN0M0 prostate cancer according to 1997 TNM classification by prostate biopsy (17 patients) or transurethral resection of the prostate (TURP) (4 patients), and underwent medical castration with a luteinizing hormone-releasing hormone (LH-RH) analogue (leuprorelin acetate 3.75 mg every 4 weeks) and chlormadinone acetate (100 mg every day). As normal controls, 8 patients (16 SV

From the Department of Urology, Furuya Hospital, Kitami; and the Department of Urology, School of Medicine, Sapporo Medical University, Sapporo, Japan

Reprint requests: Ryoji Furuya, M.D., Department of Urology, Furuya Hospital, 2-4-3 kotobuki-cho, Kitami, 090-0065, Japan.

Submitted: August 7, 2007, accepted (with revisions): November 8, 2007

0090-4295/08/$34.00
doi:10.1016/j.urology.2007.11.025

Table 1. Patients' characteristics

	Medical Castration Group	Controls	*P*-Value*
No. of patients (No. of SV)	21 (42)	8 (16)	
Median age (yr [range])	74 (67–85)	68 (64–79)	0.06
Median serum PSA (ng/mL)	12.7 (4.2–43.7)	1.0 (0.2–3.1)	<0.01
Median follow-up (mo [range])	6 (3–16)	12 (3–19)	0.03
Clinical stage (No.)	T1a (4), T1c (6) T2a (5), T2b (1) T3a (5)	T1a (8)	
Median Gleason sum (range)	7 (5–10)	5 (3–6)	<0.01

PSA, prostate-specific antigen; *SV*, seminal vesicles.

and 8 prostate) with T1aN0M0 prostate cancer after TURP were enrolled in this study. They were observed in a watchful waiting manner without any other additional treatments. Serum prostate-specific antigen (PSA) was within the normal range and there were no abnormal palpable lesions within the prostate on digital rectal examination. Table 1 lists the patients' characteristics. There were significant differences in PSA level, follow-up period and Gleason sum.

The study protocol was approved by the ethics committee and Institutional Review Board of the Kitami Medical Association. All patients were informed about the risks and benefits, and agreed to participate by written informed consent.

Transrectal Ultrasonography (TRUS) Imaging Study

We performed TRUS imaging studies using an ALOKA SSD-5000 ultrasound apparatus (ALOKA, Ltd., Tokyo, Japan) with a biplane high-resolution 5.0- to 7.5-MHz transrectal transducer. Prostate volume (in milliliters) was determined using the formula: 0.523 × anterior-posterior diameter (cm) × transverse diameter (cm) × longitudinal diameter (cm). The maximum anterior-posterior diameters of both right and left SV were measured in the transverse view. The maximum lateral diameter of the SV was measured in the longitudinal view by handling the probe parallel to the lateral diameter (Fig. 1). We determined SVV using the formula: 0.523 × (anterior-posterior diameter [cm])^2 × lateral diameter (cm). The anterior-posterior diameter of SV and SVV were chosen to be evaluation items for SV, and we usually expressed the value as mean of both SV. Every TRUS examination was performed after at least a 3-day abstinence period just in case, although it was already reported that the seminal vesicle size did not change after ejaculation.[10]

Cross-sectional Study

We cross-sectionally measured both SVV and PV in these groups using TRUS. The investigation points were pre- and post-treatment in the medical castration group and the first and second measurement in control. Measurement of PV and SV diameter and SVV was described as above.

Longitudinal Study

We prospectively assessed 7 of the 21 patients who received medical castration for more than 12 months for PSA, PV, and SVV at each period (3 to 6, 7 to 12, and 13 to 18 months).

Statistical Analysis

Statistical comparison between groups and right and left SV were done using the Mann-Whitney *U*-test. Those before and after treatment or the first and second measurements were done with the Wilcoxon signed-rank test. A *P*-value less than 0.05 was considered statistically significant.

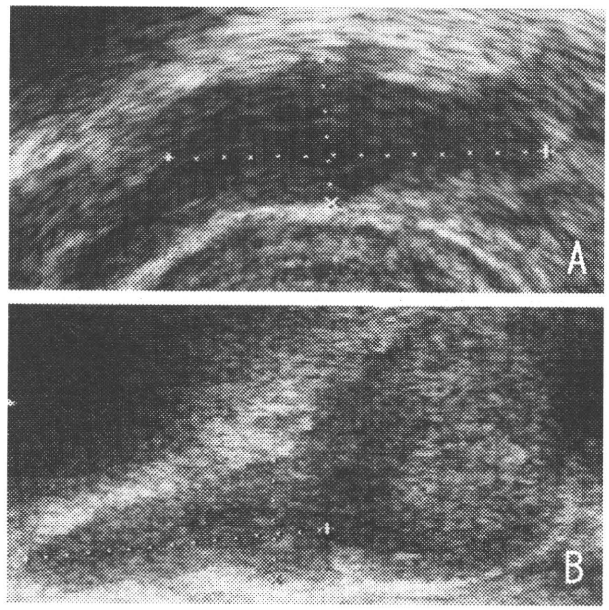

Figure 1. Demonstration of measurement of seminal vesicle with transrectal ultrasonography. **(A)** Transverse view (measurement of anterior–posterior diameter, dotted line from top to below). **(B)** Longitudinal view (measurement of lateral diameter, dotted line from left to right).

RESULTS

Figure 2 shows typical differences of seminal vesicles images before and after medical castration. The SV size was obviously reduced after medical castration.

Table 2 shows the cross-sectional results of the volume changes of the prostate and SV. We carried out the volume calculation from the TRUS results. Although the prostate volumes were significantly different for the medical castration and control groups, both PV and SVV were significantly decreased in the medical castration group at this study point, whereas those in the control group were maintained. There were no significant differences between right and left SVV and anterior-posterior diameter of SV.

In the longitudinal assessment, every parameter including mean PSA, PV, SVV, and the anterior-posterior

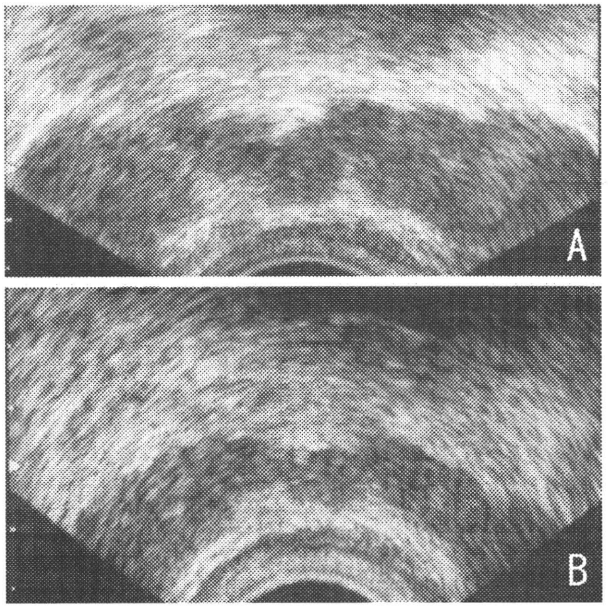

Figure 2. Representative TRUS images of seminal vesicles before and after medical castration. A 78-year-old T1cN0M0 prostate cancer patient. **(A)** Before medical castration. **(B)** At 8 months after medical castration.

diameter of SV was significantly reduced gradually up to 12 months after medical castration (Table 3). There was no significant difference between 7 and 12 months, and 13 and 18 months in these parameters except for SVV. The rates of reduction in the PV and SVV were 46.5% and 32.4% when comparing the baseline and 3 and 6 months, 27.0% and 30.4% comparing 3 and 6 months and 7 and 12 months, and −6.0% and 18.8% comparing 7 and 12 months and 13 and 18 months, respectively. The overall rates of reduction at 13 and 18 months after castration were 58.6% and 61.8% for PV and SVV, respectively.

COMMENT

There are many reports regarding the change of the prostate volume in prostate cancer patients after androgen ablation.[11–13] These reports were mostly associated with neoadjuvant hormonal therapy before external irradiation, brachytherapy, or radical prostatectomy. The rate of decrease has been reported to be about 30% to 40% after at least 3 months of androgen deprivation.

A longer period (8 months) of hormonal therapy was reported to be more beneficial for high-risk patients than short-term neoadjuvant androgen deprivation (3 months) before radiotherapy.[14] Thus, recently, neoadjuvant hormonal therapy is believed to be essential for high-risk prostate cancer patients. On the other hand, Liu *et al.* reported that long-term neoadjuvant androgen ablation before external irradiation did not increase the risk of developing gastrointestinal late toxicity.[15] Furthermore, patients with an enlarged prostate had a 2.5-fold increased risk of chronic genitourinary complications

Table 2. Cross-sectional comparison between medical castration group and controls

	Medical Castration (21 Patients, 42 SV)		Controls (8 Patients, 42 SV)	
	Pre-Tx	Post-Tx	1st (After TURP)	2nd
PV (mL)	28.4 ± 9.3*†	17.0 ± 5.3†	16.6 ± 5.7*	16.5 ± 5.3
SVV (mL)	3.5 ± 1.8†	1.9 ± 1.0†	2.5 ± 1.0	2.6 ± 1.6
	(Rt; 3.4 ± 1.6, Lt; 3.5 ± 2.1)	(Rt; 1.9 ± 0.9, Lt; 1.9 ± 1.1)	(Rt; 2.4 ± 0.8, Lt; 2.7 ± 1.3)	(Rt; 2.4 ± 0.8, Lt; 2.5 ± 1.1)
Anterior–posterior diameter of SV (mm)	11.9 ± 2.9†	8.9 ± 1.9†	10.2 ± 1.8	10.0 ± 2.0
	(Rt; 11.8 ± 2.7, Lt; 12.1 ± 3.1)	(Rt; 8.8 ± 1.8, Lt; 9.1 ± 2.0)	(Rt; 9.9 ± 1.2, Lt; 10.5 ± 2.3)	(Rt; 9.8 ± 1.8, Lt; 10.4 ± 2.2)

PV, prostate volume; *SW*, SV volume; other abbreviations as in Table 1.
Values are expressed as mean ± SEM.
* $P < 0.01$, Mann-Whitney *U*test (medical castration group versus controls).
† $P < 0.01$ Wilcoxon signed-rank test (Pre-Tx versus Post-Tx).

Table 3. Longitudinal changes of PSA, prostate size, and seminal vesicle size in the medical castration group (7 patients, 14 SV)

	Pre-Tx	3–6 mo	7–12 mo	13–18 mo
PSA (ng/mL)	11.3 ± 13.7	0.2 ± 0.2*	0.1 ± 0.1*	0.1 ± 0.1
PV (mL)	25.6 ± 8.8	13.7 ± 3.3*	10.0 ± 1.6*	10.6 ± 1.6
SVV (mL)	3.4 ± 1.4	2.3 ± 0.9*	1.6 ± 0.6*	1.3 ± 0.7*
Anterior–posterior diameter of SV (mm)	12.4 ± 2.1	9.7 ± 1.6*	8.6 ± 1.5*	8.1 ± 1.8

Abbreviations as in previous tables.
Values are expressed as mean ± SEM.
* $P < 0.05$ Wilcoxon signed-rank test (pre-Tx versus 3 to 6 months, 3 to 6 months versus 7 to 12 months, and 7 to 12 months versus 13 to 18 months).

after mixed conformal neutron and photon irradiation.[16] Thus, a small prostate has some benefits to prevent undesirable adverse effects, and neoadjuvant hormonal therapy also has a role in this. We carried out quantitative measurement of prostate and SV size in human subjects over a longer time course up to 12 months. In the current study, the size reduction of the prostate and SV continued up to 12 months, and especially marked reductions were seen up to 6 months. Together, the optimized duration of neoadjuvant hormonal therapy is considered to be at least 6 months, taking up to 12 months for the maximum effect.

There is not yet consensus as to whether the SV should be involved as a clinical target for radiotherapy for localized prostate cancer.[17,18] Kestin and colleagues reported that SV should be included if the PSA level is 10 ng/mL or more, Gleason score is 7 or more, or clinical stage is T2b or more. A total of 27% of patients with these findings exhibited SV involvement in radical prostatectomy specimens.[17] However, excluding the SV from the target volume may reduce the normal tissue reaction.[18] Thus, size reduction of SV by androgen ablation would lead to preventing undesirable complications which are common in high-risk patients with SV invasion.

In animal experiments, changes in reproductive organs, including the prostate[19–21] and SV[1–4] have been reported to be induced by androgen ablation. The changes reported include weight reduction,[1–3] cell atrophy,[1] Golgi apparatus deterioration,[2] and blood flow reduction[4] in seminal vesicles. Regarding the SV changes, as far as we know there has been only one report that the size of human SV decreases with androgen ablation, which showed that the decrease of the mean maximum horizontal area was 36% in 4 months, and it changed in parallel with the serum testosterone level.[5] The decrease was similar to our reduction rate of SVV (32.4%) between the baseline and 3 to 6 months.

In the current study, we clearly demonstrated the morphological changes of the prostate and SV with TRUS. The anterior–posterior diameter of SV has been commonly used in investigation of seminal vesicle size.[22,23] The reasons for the frequent use of anterior–posterior diameter are that it is easier to measure than lateral diameter and the value does not vary widely among technicians. The data of SVV were intended to demonstrate the reduction easily. Measurement of the lateral diameter of SV is technically difficult; however, our measurement, done by handling the probe parallel to the lateral diameter in the longitudinal view, has the possibility of providing a precise value.

A major limitation of our study is that it was designed as a prospective study rather than as a randomized control one; in other words, all patients in the control group underwent TURP. This might lead to bias especially for the prostate volume, which might have reduced the volume of shrinkage found during this study period. SV volume technically was not influenced, although there might have been damage to the ejaculatory duct, which might have caused the seminal fluid to leak. To eliminate these limitations, we should consider a randomized control study using watchful waiting patients or benign prostatic hyperplasia as controls.

CONCLUSIONS

In conclusion, the current study clearly demonstrated the morphological changes of the prostate and SV quantitatively. It is proposed that the duration of hormonal therapy as neoadjuvant treatment before radiation be at least 6 months, and as long as 12 months for the maximum effect, because most dynamic changes were seen in this period. We should confirm the clinical benefits of this duration on high-risk prostate cancer patients in the near future.

References

1. Bruengger A, Mariotti A, Rohr HP, *et al:* Androgen and estrogen effect on guinea pig seminal vesicle muscle: a combined stereological and biochemical study. Prostate **9:** 303-310, 1986.
2. Tam CC, Wong YC, and Tang F: Further regression of seminal vesicles of castrated guinea pig by administration of cyproterone acetate. Acta Anat (Basel) **124:** 65-73, 1985.
3. Godowicz B: Weight of seminal vesicles and size of penis papillae in castrated mice depending on a dose of testosterone propionate. Folia Biol (Krakow) **17:** 333-340, 1969.
4. Ono Y, Suzuki K, Kashiwagi B, *et al:* Role of androgen on blood flow and capillary structure in rat seminal vesicles. Tohoku J Exp Med **202:** 193-201, 2004.
5. Terasaki T, Kojima M, Kamoi K, *et al:* Effect of LHRH analog on the seminal vesicles evaluated by transrectal sonography. Prostate **23:** 115-121, 1993.
6. Zietman AL, Chung CS, Coen JJ, *et al:* 10-year outcome for men with localized prostate cancer treated with external radiation therapy: results of a cohort study. J Urol **171:** 210-214, 2004.

7. Takahashi A, Yanase M, Masumori N, *et al:* External beam radiation monotherapy for localized or locally advanced prostate cancer. Jpn J Clin Oncol **33:** 73-77, 2003.
8. Bolla M: Adjuvant hormonal treatment with radiotherapy for locally advanced prostate cancer. Eur Urol **35(Suppl 1):** 23-25; discussion 26, 1999.
9. Valicenti RK, Winter K, Cox JD, *et al:* RTOG 94-06: is the addition of neoadjuvant hormonal therapy to dose-escalated 3D conformal radiation therapy for prostate cancer associated with treatment toxicity? Int J Radiat Oncol Biol Phys **57:** 614-620, 2003.
10. Hernandez AD, Urry RL, Smith JA Jr: Ultrasonographic characteristics of the seminal vesicles after ejaculation. J Urol **144:** 1380-1382, 1990.
11. Gleave ME, Goldenberg SL, Chin JL, *et al:* Randomized comparative study of 3 versus 8-month neoadjuvant hormonal therapy before radical prostatectomy: biochemical and pathological effects. J Urol **166:** 500-506; discussion 506–507, 2001.
12. Kucway R, Vicini F, Huang R, *et al:* Prostate volume reduction with androgen deprivation therapy before interstitial brachytherapy. J Urol **167:** 2443-2447, 2002.
13. Solhjem MC, Davis BJ, Pisansky TM, *et al:* Prostate volume before and after permanent prostate brachytherapy in patients receiving neoadjuvant androgen suppression. Cancer J **10:** 343-348, 2004.
14. Crook J, Ludgate C, Malone S, *et al:* Report of a multicenter Canadian phase III randomized trial of 3 months vs. 8 months neoadjuvant androgen deprivation before standard-dose radiotherapy for clinically localized prostate cancer. Int J Radiat Oncol Biol Phys **60:** 15-23, 2004.
15. Liu M, Pickles T, Agranovich A, *et al:* Impact of neoadjuvant androgen ablation and other factors on late toxicity after external beam prostate radiotherapy. Int J Radiat Oncol Biol Phys **58:** 59-67, 2004.
16. Forman JD, Keole S, Bolton S, *et al:* Association of prostate size with urinary morbidity following mixed conformal neutron and photon irradiation. Int J Radiat Oncol Biol Phys **45:** 871-875, 1999.
17. Kestin L, Goldstein N, Vicini F, *et al:* Treatment of prostate cancer with radiotherapy: should the entire seminal vesicles be included in the clinical target volume? Int J Radiat Oncol Biol Phys **54:** 686-697, 2002.
18. Marks LB, and Anscher MS: Radiotherapy for prostate cancer: should the seminal vesicles be considered target? Int J Radiat Oncol Biol Phys **24:** 435-440, 1992.
19. Kiplesund KM, Halgunset J, Fjosne HE, *et al:* Light microscopic morphometric analysis of castration effects in the different lobes of the rat prostate. Prostate **13:** 221-232, 1988.
20. Donjacour AA, and Cunha GR: The effect of androgen deprivation on branching morphogenesis in the mouse prostate. Dev Biol **128:** 1-14, 1988.
21. Habenicht UF, Schneider MR, and el Etreby MF: Induction of chemical castration in male rats by a new long-acting LHRH-antagonist. Prostate **17:** 69-83, 1990.
22. Littrup PJ, Lee F, McLeary RD, *et al:* Transrectal US of the seminal vesicles and ejaculatory ducts: clinical correlation. Radiology **168:** 625-628, 1988.
23. Kuligowska E, Baker CE, and Oates RD: Male infertility: role of transrectal US in diagnosis and management. Radiology **185:** 353-360, 1992.

TRIM68 Regulates Ligand-Dependent Transcription of Androgen Receptor in Prostate Cancer Cells

Naoto Miyajima,[1,2] Satoru Maruyama,[1,2] Miyuki Bohgaki,[1] Satoshi Kano,[1] Masahiko Shigemura,[3] Nobuo Shinohara,[2] Katsuya Nonomura,[2] and Shigetsugu Hatakeyama[1]

Departments of [1]Biochemistry and [2]Urology, and [3]First Department of Medicine, Hokkaido University Graduate School of Medicine, Sapporo, Japan

Abstract

The androgen receptor (AR) is a transcription factor belonging to the family of nuclear receptors that mediate the action of androgen. AR plays an important role in normal development of the prostate, as well as in the progression of prostate cancer. AR is regulated by several posttranslational modifications, including phosphorylation, acetylation, and ubiquitination. In this study, we found that the putative E3 ubiquitin ligase TRIM68, which is preferentially expressed in prostate cancer cells, interacts with AR and enhances transcriptional activity of the AR in the presence of dihydrotestosterone. We also found that TRIM68 functionally interacts with TIP60 and p300, which act as coactivators of AR, and synergizes in the transactivation of AR. Overexpression of TRIM68 in prostate cancer cells caused an increase in secretion of prostate-specific antigen (PSA), one of the most reliable diagnostic markers for prostate cancer, whereas knockdown of TRIM68 attenuated the secretion of PSA and inhibited cell growth and colony-forming ability. Moreover, we showed that TRIM68 expression is significantly up-regulated in human prostate cancers compared with the expression in adjacent normal tissues. These results indicate that TRIM68 functions as a cofactor for AR-mediated transcription and is likely to be a novel diagnostic tool and a potentially therapeutic target for prostate cancer. [Cancer Res 2008;68(9):3486–94]

Introduction

Prostate cancer is the most frequently diagnosed malignancy and is the second leading cause of cancer deaths among men in the United States (1). Prostate cancer is a hormonally regulated malignancy, and androgen receptor (AR) plays an important role in disease progression (2). One of the most troubling aspects of prostate cancer progression is the conversion from an androgen-dependent state to an androgen ablation–resistant state, which, at present, defies any effective treatment (3). In majority of end-stage hormone-refractory tumors, AR continues to be expressed and seems to be activated under androgen ablation conditions. Elucidation of the mechanism of AR activation is essential for understanding process of the prostate cancer progression and for identifying possible targets for intervention (4). AR mediates androgen action as a transcriptional factor in collaboration with a number of coregulators. AR up-regulates or down-regulates target gene expressions, depending on coactivators or corepressors (5, 6). Furthermore, activities of AR and coregulators are regulated by posttranslational modifications, such as methylation, phosphorylation, acetylation, and ubiquitination (7–10). However, little is known about the contribution of such processes to AR function.

Ubiquitination is a versatile posttranslational modification mechanism used by eukaryotic cells. The ubiquitin-proteasome pathway involves ubiquitin modification of substrates and sequential degradation by the proteasome (11). Ubiquitin conjugation is catalyzed by ubiquitin-activating enzyme (E1), ubiquitin-conjugating enzyme (E2), and ubiquitin ligase (E3; ref. 12). E3 is a scaffold protein that mediates between the ubiquitin-linked E2 and the substrate. The resulting covalent ubiquitin ligations form polyubiquitinated conjugates that are rapidly detected and degraded by 26S proteasome (13). E3 is thought to be most directly responsible for substrate recognition. E3 ubiquitin ligases thus far identified include members of the homologous to E6-AP carboxyl terminus (HECT), RING finger, and U-box protein families (14–16).

TRIM68 is a member of the tripartite motif-containing protein (TRIM) family defined by the presence of a common domain structure composed of a RING finger, a B-box, and a coiled-coil motif (17). In addition to these motifs, TRIM68 possesses a carboxy-terminal PRY/SPRY domain. TRIM family proteins are involved in a broad range of biological processes, and consistently, their alterations result in diverse pathologic conditions, such as genetic diseases, viral infection, and cancer development (18). It has been reported that TRIM68 is one of the autoantigens associated with Sjögren's syndrome and is a new diagnostic marker for Sjögren's syndrome (19). However, the function of TRIM68 has not been elucidated. Recently, TRIM68 has also been shown to be highly expressed in the prostate compared with its expression in other normal tissues. TRIM21, which is structurally similar to TRIM68 and is also one of the autoantigens associated with Sjögren's syndrome, has been found to bind DNA and has been suggested to act as a transcription factor regulating gene expression (20, 21). TRIM21 has also been shown to be involved in cellular proliferation and cell death (22). Given the highly prostate-specific expression pattern of TRIM68 and the transcriptional function of its related protein, we hypothesized that TRIM68 plays a role in AR-dependent transcription.

In this study, we obtained evidence that TRIM68 is a novel AR-interacting protein and acts as a coactivator of AR, depending on its ubiquitin ligase activity. Furthermore, knockdown of endogenous TRIM68 expression by RNA interference (RNAi) results in suppression of the oncogenic properties of prostate cancer cells. In addition, we found that TRIM68 is significantly up-regulated in human prostate cancers, suggesting that TRIM68 is likely to be a novel diagnostic tool for prostate cancer.

Requests for reprints: Shigetsugu Hatakeyama, Department of Biochemistry, Hokkaido University Graduate School of Medicine, N15, W7, Kita-ku, Sapporo, Hokkaido 060-8638, Japan. Phone: 81-11-706-5899; Fax: 81-11-706-5169; E-mail: hatas@med.hokudai.ac.jp.

doi:10.1158/0008-5472.CAN-07-6059

Materials and Methods

Cell culture. Prostate cancer cell lines LNCaP-FGC, CWR22Rv1, and PC3 were obtained from the American Type Culture Collection. LNCaP and CWR22Rv1 were maintained under an atmosphere of 5% CO_2 at 37°C in RPMI 1640 (Sigma Chemical Co.) supplemented with 10% fetal bovine serum (FBS; Life Technologies Bethesda Research Laboratories). PC3 and HEK293T cell lines were cultured under the same conditions in DMEM (Sigma) with 10% FBS.

Cloning of cDNAs and plasmid construction. Human TRIM68 cDNA was amplified by PCR from HeLa cDNA (Clontech Laboratories, Inc.). The resulting fragment containing the human TRIM68 cDNA was ligated into the pCR3 vector (Invitrogen) with a FLAG tag and into the pFastBacHT vector (Invitrogen). Human AR cDNA was kindly provided by Dr. Sobue (Nagoya University). Deletion mutants of AR cDNA were generated by PCR. Human TIP60 cDNA was kindly provided by Dr. Ikura (Tohoku University).

Recombinant proteins, antibodies, and reagents. His-tagged TRIM68 was expressed in the Sf9 insect cell line using a baculovirus protein expression system (Invitrogen). The recombinant TRIM68 protein was used as immunogen in rabbits. A rabbit polyclonal anti-TRIM68 antibody was generated and then affinity-purified using a recombinant TRIM68-conjugated Sepharose 4B column. Other antibodies used were as follows: mouse monoclonal anti-HA (HA.11/16B12, Covance Research Products), mouse monoclonal anti-FLAG (M5, Sigma), mouse monoclonal anti-ubiquitin (P4D1, Santa Cruz Biotechnology), goat polyclonal anti–prostate-specific antigen (PSA; Santa Cruz), mouse monoclonal anti-AR (Santa Cruz), and mouse monoclonal anti–α-tubulin (Zymed Laboratories). Dihydrotestosterone, dexamethasone, and 17β-estradiol were purchased from Sigma.

Ubiquitination assay. *In vitro* ubiquitination assays were performed as previously described (16). In brief, reaction mixtures containing 4 μg of the recombinant TRIM68 with 0.1 μg recombinant E1 (Boston Biomedica), 1 μg recombinant E2s, 0.5 unit phosphocreatine kinase, 1 μg ubiquitin (Sigma), 25 mmol/L Tris-HCl (pH 7.5), 120 mmol/L NaCl, 2 mmol/L ATP, 1 mmol/L $MgCl_2$, 0.3 mmol/L DTT, and 1 mmol/L creatine phosphate were incubated for 3 h at 30°C. The reaction was terminated by the addition of SDS sample buffer containing 4% β-mercaptoethanol and heating at 95°C for 5 min. Samples were subjected to immunoblotting with anti-ubiquitin and anti-TRIM68 antibodies.

Transfection, immunoprecipitation, and immunoblot analysis. HEK293T cells were transfected by the calcium phosphate method. After 48 h, the cells were lysed in a solution containing 50 mmol/L Tris-HCl (pH 7.4), 150 mmol/L NaCl, 1% Nonidet P-40, leupeptin (10 μg/mL), 1 mmol/L phenylmethylsulfonyl fluoride, 400 μmol/L Na_3VO_4, 400 μmol/L EDTA, 10 mmol/L NaF, and 10 mmol/L sodium PPi. The cell lysates were centrifuged at 16,000 × *g* for 10 min at 4°C, and the resulting supernatant was incubated with antibodies for 2 h at 4°C. Protein A-Sepharose (Amersham Pharmacia) that had been equilibrated with the same solution was added to the mixture, and then the mixture was rotated for 1 h at 4°C. The resin was separated by centrifugation, washed five times with ice-cold lysis buffer, and then boiled in SDS sample buffer. Immunoblot analysis was performed with primary antibodies, horseradish peroxidase–conjugated antibodies to mouse or rabbit IgG (1:10,000 dilution; Promega), and an enhanced chemiluminescence system (Amersham Pharmacia).

Establishment of stable transfectants by using a retrovirus expression system. Complementary DNAs were subcloned into pMX-puro (kindly provided by T. Kitamura, Tokyo University), the resulting vectors were used to transfect Plat A cells, and then recombinant retroviruses were generated (23). LNCaP cells were infected with the recombinant retroviruses and selected in medium containing puromycin (2 μg/mL; Sigma).

RNAi. The pMX-puro II vector in which the U3 portion of the 3′ long terminal repeat was deleted was kindly provided by Dr. T. Kamura (Nagoya University; ref. 24). The hairpin sequences specific for human TRIM68 mRNAs corresponded to nucleotides 329 to 349 (siTRIM68-1) and 796 to 816 (siTRIM68-2) of the respective coding regions. The hairpin sequences specific for enhanced green fluorescent protein (GFP; Clontech) mRNA were used as a control. Recombinant retroviruses were generated and used to infect LNCaP cells as described above. After selection in medium containing puromycin (2 μg/mL), the resulting cell lines were checked by immunoblot analysis with anti-TRIM68 antibody.

Dual-luciferase assay. Cells were seeded in 24-well plates at 1×10^5 per well (LNCaP) or 5×10^4 per well (PC3 and CWR22Rv1) and incubated at 37°C with 5% CO_2 for 24 h. The mouse mammary tumor virus-luciferase (MMTV-Luc) reporter plasmid and the pRL-TK *Renilla* luciferase plasmid (Promega) were transfected with the TRIM68 expression vector into LNCaP and CWR22Rv1 cells or with the AR expression vector into PC3 cells using Fugene HD reagent (Roche). Estrogen-response element reporter plasmid (ERE-Luc) was used for the estrogen receptor (ER)–luciferase assay. Transfected cells were incubated in 10% charcoal–treated FBS (Equitech-Bio) medium for 48 h and then washed and treated with or without 10 nmol/L dihydrotestosterone for 24 h, harvested, and assayed for luciferase activity with a Dual-Luciferase Reporter Assay System (Promega). The luminescence was quantified with a luminometer (Promega).

PSA expression and secretion assays. LNCaP cell lines were seeded in six-well plates and incubated in 10% charcoal–treated FBS medium for 48 h and then washed and treated with or without 10 nmol/L dihydrotestosterone for 24 h. The cells were lysed and subjected to immunoblotting with anti-PSA antibody. Cell culture media were collected and assayed for PSA concentration by ELISA analysis using a TOSOH II PA monoclonal immunoenzyme assay kit.

Cell proliferation assay. LNCaP cell lines were incubated in 10% charcoal–treated FBS medium for 48 h and then plated into 96-well plates at 5,000 per well in 100 μL medium. Cells were treated with 10 nmol/L dihydrotestosterone and refed with fresh medium containing dihydrotestosterone every 2 d. MTS cell proliferation assay was performed using CellTiter 96 one solution (Promega) according to the manufacturer's instructions.

Colony formation assay in soft agar. LNCaP cells were plated at a density of 1×10^4 cells in 60-mm dishes containing 0.4% top low-melting agarose and 0.5% bottom low-melting agarose medium. Colonies with a diameter of >0.1 mm were counted after 3 wk.

Reverse transcription and real-time quantitative PCR. Total RNA (3 μg) isolated from various cell lines, human prostate cancers, and adjacent normal tissues with the use of TRI Reagent (Sigma) was subjected to reverse transcription with MMLV Reverse Transcriptase (Invitrogen). The resulting cDNA was subjected to real-time quantitative PCR by TaqMan gene expression assays (Applied Biosystems) following the manufacturer's instructions. The assays were performed with a TRIM68-specific TaqMan probe and primers (synthesized by Applied Biosystems) in an ABI-PRISM 7000 Sequence Detection System (Applied Biosystems). TATA box-binding protein (TBP) was selected as an internal control to normalize the expression levels. Each sample was tested in triplicate.

Human tissue samples. Tissues from 35 cases of primary prostate cancer were surgically resected by radical prostatectomy. Written informed consent was obtained from each patient before surgery. The excised samples from tumor and adjacent normal tissues were obtained within 1 h after the operation. All excised tissues were immediately placed in liquid nitrogen and stored at −80°C until further analysis. Samples were then manually microdissected from frozen sections on microscope and histologically confirmed to be highly homogeneous cancer tissues by H&E staining of step sections.

Immunohistochemical analysis. Tissues were fixed in 4% formaldehyde for 3 d and then embedded in paraffin. Paraffin-embedded sections (3-μm thick) were mounted on silane-treated slides. After drying overnight at 37°C, paraffin was removed from the sections with xylene, and they were then rehydrated with a graded series of ethanol solutions. The tissues were then subjected to immunohistochemical staining with an antibody to TRIM68 (5 μg/mL) by a streptavidin-biotin immunoperoxidase method using an immunohistochemical detection kit (Vectastain Elite; Vector) and diaminobenzidine as a chromogen (Wako) according to the manufacturer's instructions. Immunoreactivity was semiquantitatively classified. Two independent investigators reviewed and scored slides observed under a microscope by categorizing staining intensity of characteristic staining cells as negative, weak, medium, or strong (scored as 0–3). The final score was

obtained by multiplying the percentage of positive cells by the intensity score with an estimated score range of 0 to 300.

Statistical analysis. We used the unpaired Student's *t* test and the Mann-Whitney *U* test to determine statistical significance of experimental data.

Results

TRIM68 has a ubiquitin ligase activity and is predominantly expressed in the prostate cancer cell line LNCaP. TRIM68 has a RING finger domain at its NH_2 terminus and belongs to the TRIM family of proteins, some of which have been reported to be E3 ubiquitin ligases (18). To determine whether TRIM68 actually mediates an E3 ligase activity, we generated recombinant TRIM68 protein by using a baculovirus expression system and performed an *in vitro* ubiquitination assays with various combinations. Immunoblot analysis using an anti-ubiquitin antibody revealed that TRIM68 exhibits ubiquitination activity only in the presence of E1, E2 (Ubc4), ubiquitin, ATP, and TRIM68 (Fig. 1*A*, *top*). The lack of any of these components prevented autoubiquitination of TRIM68. In addition, an *in vitro* ubiquitination assay using anti-TRIM68 antibody showed that TRIM68 has an autoubiquitination activity (Fig. 1*A*, *bottom*). These findings indicate that TRIM68 is a bona fide E3 ligase. To further investigate the region of TRIM68 responsible for ubiquitination, we generated a deletion mutant lacking a RING finger domain (ΔRING) of TRIM68 and then performed an *in vitro* ubiquitination assay (Fig. 1*B*). The *in vitro* ubiquitination assay showed that the deletion mutant has no E3 ligase activity, indicating that the RING finger domain is indispensable for E3 ubiquitin ligase activity of TRIM68.

To study the expression profile of TRIM68, we measured TRIM68 mRNA levels in various human cell lines of different origins by using real-time quantitative reverse transcription–PCR (RT-PCR). The gene expression of TRIM68 was found predominantly in the prostate cancer cell line LNCaP compared with its expression in other cell lines, including the prostate cancer cell lines CWR22Rv1 and PC3, B-cell lymphoma cell line Namalwa, embryonic kidney cell line 293, breast cancer cell lines T47D and MCF7, uterine epithelial carcinoma cell line HeLa, neuroblastoma cell line SH-SY5Y, and hepatocellular carcinoma cell line HepG2 (Fig. 1*C*). Next, we compared the protein levels of TRIM68 by immunoblotting in hormone-related cancer cell lines, including LNCaP, 22Rv1, PC3, T47D, and MCF7. Consistent with the observed mRNA expression pattern, TRIM68 protein was found to be abundantly expressed in the prostate cancer cell line LNCaP compared with its expression in other cell lines (Fig. 1*D*).

Interaction between TRIM68 and AR. Given that TRIM68 is highly expressed in the androgen-responsive prostate cancer cell line LNCaP, we hypothesized that TRIM68 is associated with prostate cancer and particularly the AR signaling pathway. To test the possibility, we verified interaction between endogenous TRIM68 and AR in LNCaP cells by immunoprecipitation using antibodies to TRIM68 and AR (Fig. 2*A*). Furthermore, to determine the domain of AR that interacts with TRIM68, deletion mutants of AR were constructed for *in vivo* binding assays (Fig. 2*B*). HA-tagged AR mutants and FLAG-tagged TRIM68 were expressed in HEK293T cells, and the cell lysates were subjected to immunoprecipitation with anti-FLAG antibody. The results showed that AR-L, including the ligand-binding domain, was coprecipitated with TRIM68 but AR-ND, including the amino-terminal domain and DNA-binding domain, was not, suggesting that the ligand-binding domain is responsible for interaction with TRIM68 (Fig. 2*C*).

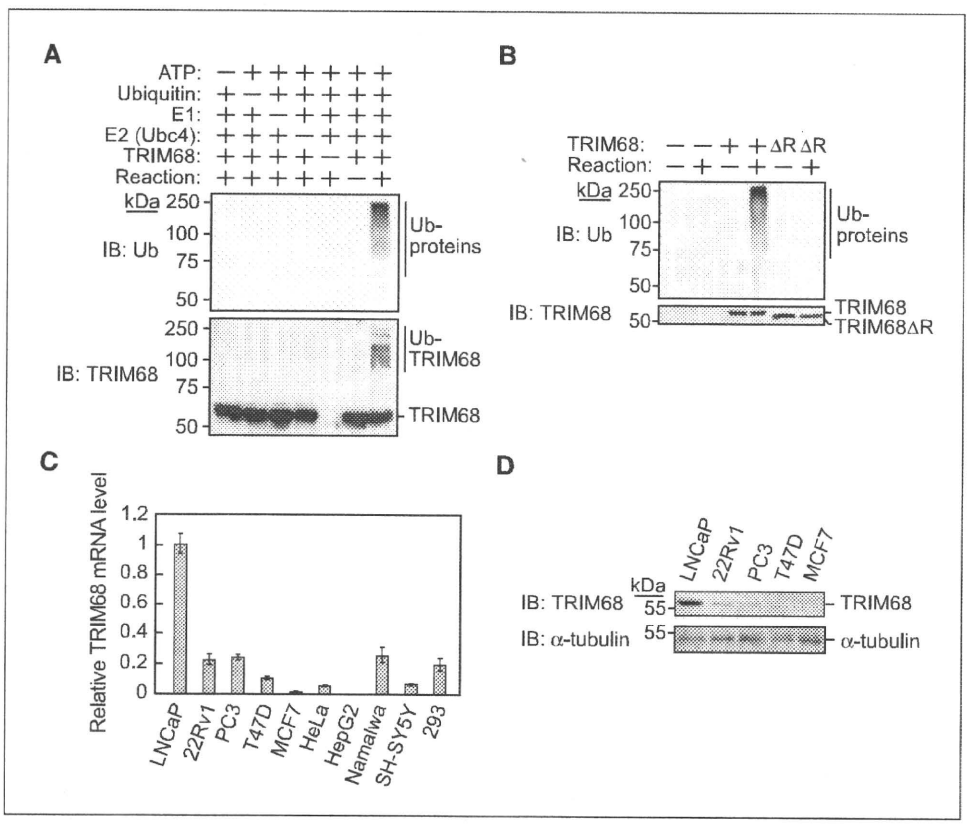

Figure 1. Ubiquitin ligase TRIM68 is predominantly expressed in prostate cancer LNCaP cells. *A*, ATP-dependent, E1-dependent, and E2-dependent ubiquitin ligase activity of TRIM68. An *in vitro* ubiquitination assay was performed with the indicated combinations of ATP, ubiquitin, E1, E2 (Ubc4), and TRIM68. The reaction mixtures were also subjected to immunoblot analysis with antibodies to ubiquitin (*top*) and TRIM68 (*bottom*). *B*, RING finger domain is indispensable for ubiquitin ligase activity of TRIM68. An *in vitro* ubiquitination assay was performed with equimolar amounts of TRIM68 derivatives (TRIM68 and TRIM68ΔR) in the presence of ATP, E1, and E2 (Ubc4). The reaction mixtures were also subjected to immunoblot analysis with antibodies to ubiquitin (*top*) and TRIM68 (*bottom*). *C*, quantitative analysis of TRIM68 transcript in various cell lines. TRIM68 mRNA expression levels in various human cell lines of different origins were quantified by real-time quantitative RT-PCR. The expression level of TRIM68 mRNA was normalized to that of TBP mRNA. The expression level of TRIM68 mRNA in LNCaP cells was defined as 1. *Columns*, mean of values from three independent experiments; *bars*, SD. *D*, TRIM68 protein expression in sex hormone–related cancer cell lines. Cell lysates from prostate or breast cancer cell lines were subjected to immunoblot analysis with anti-TRIM68 and anti–α-tubulin antibodies. Prostate cancer cell lines: LNCaP, 22Rv1, and PC3; breast cancer cell lines: T47D and MCF7.